



H₂O subduction beyond arcs

Bradley R. Hacker

*Department of Earth Science, University of California, Santa Barbara, California 93109-9630, USA
(hacker@geol.ucsb.edu)*

[1] The amount of H₂O subducted to postarc depths dictates such disparate factors as the generation of arc and back-arc magmas, the rheology of the mantle wedge and slab, and the global circulation of H₂O. *Perple_X* was used to calculate phase diagrams and rock physical properties for pressures of 0.5–4.0 GPa and temperatures of 300–900°C for a range of bulk compositions appropriate to subduction zones. These data were merged with global subduction zone rock fluxes to generate a model for global H₂O flux to postarc depths. For metasomatized igneous rocks, subducted H₂O scales with bulk rock K₂O in hot slabs. Metasomatized ultramafic rocks behave similarly in cold slabs, but in hot slabs carry no H₂O to magma generation depths because they lack K₂O. Chert and carbonate are responsible for minimal H₂O subduction, whereas clay-rich and terrigenous sediments stabilize several hydrous phases at low temperature, resulting in significant postarc slab H₂O flux in cold and hot slabs. Continental crust also subducts much H₂O in cold slabs because of the stability of lawsonite and phengite; in hot slabs it is phengite that carries the bulk of this H₂O to postarc depth. All told, the postarc flux of H₂O in cold slabs is dominated by terrigenous sediment and the igneous lower crust and mantle and is proportional to bulk rock H₂O. In contrast, in hot slabs the major contributors of postarc slab H₂O are metasomatized volcanic rocks and subducted continental crust, with the amount of postarc slab H₂O scaling with K₂O. The Andes and Java-Sumatra-Andaman slabs are the principal suppliers of pelagic and terrigenous sediment hosted H₂O to postarc depths, respectively. The Chile and Solomon arcs contribute the greatest H₂O flux from subducted continental and oceanic forearc, respectively. The Andean arc has the greatest H₂O flux provided through subduction of hydrated ocean crust and mantle. No correlation was observed between postarc slab H₂O flux and slab seismicity.

Components: 11,646 words, 12 figures, 4 tables.

Keywords: subduction; H₂O; water; flux; global.

Index Terms: 1031 Geochemistry: Subduction zone processes (3060, 3613, 8170, 8413); 3612 Mineralogy and Petrology: Reactions and phase equilibria (1012, 8412).

Received 31 May 2007; **Revised** 26 October 2007; **Accepted** 7 December 2007; **Published** 5 March 2008.

Hacker, B. R. (2008), H₂O subduction beyond arcs, *Geochem. Geophys. Geosyst.*, 9, Q03001, doi:10.1029/2007GC001707.

1. Introduction

[2] The amount of H₂O carried in subducting slabs to depths greater than arc magma generation depths (henceforth “postarc” slab H₂O flux) dictates such disparate factors as the global circulation of H₂O

between the hydrosphere and the solid Earth, the rheology of the mantle and slab; conversely, H₂O that leaves the slab at shallower depths influences the rheology of the mantle wedge and arc volcanism. The purpose of this paper is to determine semiquantitatively the amount of H₂O carried in subducting

Table 1. Modeled Bulk Compositions^a

	SiO ₂	TiO ₂	Al ₂ O ₃	FeO	MnO	MgO	CaO	Na ₂ O	K ₂ O	H ₂ O ^b	H ₂ O ^c	CO ₂	Cold Slab ^d	Hot Slab ^e
MORB	50.6	1.5	15.7	10.6		7.6	11.1	2.6	0.2	5.3	n.m.	0.0	2.5	0.07
Gabbro	50.6	0.9	16.1	6.2		9.2	12.5	2.8	0.1	5.2	n.m.	0.0	3.5	0.02
Troctolite 209-1275B-6R-1, 61-64	40.7	0.2	3.8	9.2		37.6	5.9	0.1	0.1	7.7	8.5	3.2	7.7	0.05
417D22	43.1	1.2	13.9	8.5		5.8	15.5	1.9	0.8	4.5	2.1	6.1	3.8	0.3
418A15	42.2	1.0	14.6	7.5		6.5	15.6	2.1	0.6	5.5	2.2	6.7	3.9	0.2
418A73	48.1	1.2	15.3	10.2		8.1	11.0	1.9	0.2	5.9	2.7	0.4	4	0.06
VCLtop	27.2	0.6	8.3	7.0		3.6	26.6	0.9	1.8	3.3	3.4	19.7	2.3	0.7
417A32	45.9	1.5	16.6	10.5		5.3	9.8	2.4	1.6	5.7	4.5	1.5	3.4	0.7
417A24	44.8	1.5	16.1	11.2		3.4	7.6	1.4	4.3	5.4	4.9	3.4	4	1.7
Ca-Al rock DSDP037-0332B-022-003/3-5	46.6	0.9	17.3	10.6		5.3	15.6	2.5	0.3	3.9	4.0	0.0	2	0.1
Epidosite	50.3	0.4	18.3	8.3		1.2	17.7	0.1	0.0	6.3	n.m.	0.0	6.3	0.3
DMM, depleted MORB mantle	44.7	0.1	4.0	8.2		38.7	3.2	0.2	0.0	12.0	n.m.	0.0	11.6	0.02
Shaka altered peridotite 63-19	52.9	0.1	2.7	8.6		32.3	2.3	0.2	0.0	8.3	5.8	0.0	8	0
Orcadas altered peridotite 58-9B	47.9	0.2	2.7	7.7		37.1	4.3	0.3	0.0	10.0	5.9	0.1	5.5	0
Mariana chert	88.7	0.1	2.3	1.3	0.3	0.7	0.4	0.5	0.6	0.8	5.0	0.0	0.8	0.2
Mariana clay	49.8	0.6	14.7	7.3	2.1	3.1	3.5	3.1	3.6	6.5	10.4	0.0	4	1.5
Guatemala carbonate	13.3	0.0	0.7	3.7		1.3	44.5	0.4	0.3	0.5	1.0	34.5	0.5	0.1
Antilles terrigenous	55.2	0.9	20.8	6.0	0.1	2.2	0.5	0.6	3.0	5.2	8.7	0.0	5.2	1.2
Biotite zone pelite	60.8	0.8	16.9	7.0	0.1	3.4	1.2	1.7	3.7	5.9	3.1	0.0	2.5	1.5
UHP gneiss (J2803N31)	74.7	0.0	12.8	1.8	0.0	0.3	1.1	3.2	5.8	0.8	n.m.	0.0	0.9	0.9

^a See figure captions for references.

^b H₂O content at saturation.

^c Measured H₂O content of rock (“n.m.” means not measured).

^d H₂O content at 4 GPa in cold slab.

slabs to postarc depths, in both individual subduction zones and globally, by calculating phase diagrams for subducting bulk rock compositions (Table 1) and rock fluxes for subduction zones. This paper builds on a host of earlier studies, cited below, that have addressed related topics. Specific questions to be addressed include the following: (1) What kinds of rocks are best suited for carrying H₂O to postarc depths in cold slabs and hot slabs? (2) What are the relative contributions of different rock types to the postarc slab H₂O flux in specific subduction zones and globally? (3) What are the relative contributions of different subduction processes (i.e., “normal” oceanic subduction, subduction erosion, continental subduction) to the postarc slab H₂O flux in specific subduction zones and globally? (4) Which subduction zones dominate the global postarc slab H₂O flux, and why? (5) What correlations exist between postarc slab H₂O flux and seismicity in subduction zones? First I examine the phase relations of the relevant rock types, and then use those phase diagrams in conjunction with subduction zone parameters to calculate postarc slab H₂O flux.

2. Phase Diagram Calculation

[3] The amount of H₂O stable in each rock type as a function of P, T, and initial H₂O content was

determined using the program *Perple_X* [Connolly and Petri, 2002; Connolly, 2005], following the approach used by Connolly et al. [Kerrick and Connolly, 2001a, 2001b; Connolly and Kerrick, 2002; Rüpke et al., 2004] (Table 2). This paper diverges from these earlier efforts by considering a broader range of bulk compositions more representative of the variety of rocks being subducted by calculating the flux for each subduction zone individually, and by including the effects of subduction erosion and continental collisions.

[4] A pressure range of 0.5–4.0 GPa, corresponding to depths of ~15 to 120–135 km, was modeled. Depths shallower than ~15 km were ignored under the assumption that the H₂O cycle in the slab at such depths is dominated by the expulsion of pore fluid. Depths of 120–135 km were the maximum considered because this approximates the depth of slabs beneath arc volcanoes [Syracuse and Abers, 2006]; the focus in this paper is on the subduction of H₂O to greater depths. A restricted temperature range of 300–900°C was modeled, encompassing the conditions calculated to pertain to subduction zones over the depth range of interest. Melting was ignored; thus the calculations strictly apply only to subsolidus conditions. Complete sample-scale equilibrium was assumed, although, in Earth, metastability is the rule at low temperature and intra-

Table 2. Perple_X Activity Models Used

Abbreviation	Mineral	Solution Model
Anth	Fe-Mg amphibole	ideal
Atg	antigorite	ideal
B	brucite	ideal
Bio(HP)	biotite	<i>Powell and Holland</i> [1999]
Carp	carpholite	ideal
Chl(HP)	chlorite	<i>Holland et al.</i> [1998]
Chum	clinochumite	ideal
Cpx(HP)	clinopyroxene	<i>Holland and Powell</i> [1996]
Ctd(HP)	chloritoid	<i>White et al.</i> [2000]
Do(HP)	dolomite	<i>Holland and Powell</i> [1998]
F	fluid	<i>Connolly and Trommsdorff</i> [1991]
feldspar	feldspar	<i>Fuhrman and Lindsley</i> [1988]
GlTrTsPg	Na-Ca amphibole	<i>Wei and Powell</i> [2003] and <i>White et al.</i> [2003]
Gt(HP)	garnet	<i>Holland and Powell</i> [1998]
M(HP)	magnesite	<i>Holland and Powell</i> [1998]
O(HP)	olivine	<i>Holland and Powell</i> [1998]
Omph(HP)	clinopyroxene	<i>Holland and Powell</i> [1996]
Opx(HP)	orthopyroxene	<i>Holland and Powell</i> [1996]
Pa	Na-white mica	<i>Chatterjee and Froese</i> [1975]
Pheng(HP)	K-white mica	“parameters from Thermocalc”
Pl(h)	plagioclase	<i>Newton et al.</i> [1980]
San	K-feldspar	<i>Thompson and Hovis</i> [1979]
Sp(HP)	spinel	<i>Holland and Powell</i> [1998]
St(HP)	staurolite	“parameters from Thermocalc”
T	talc	ideal

crystalline diffusion effectively fractionates crystal cores from the bulk rock composition.

[5] A wide range of bulk compositions representative of the broad range of materials subducted were modeled (Table 1). (1) Unmetasomatized oceanic igneous rocks were modeled using a MORB and a gabbro bulk composition. (“Metasomatized” and “metasomatism” are used to denote changes in bulk composition that involve the gain or loss of elements other than H₂O. “(De)hydration” is used to denote the (loss) gain of H₂O only. Combinations of these terms are possible such that a rock may be hydrated and unmetasomatized (i.e., unchanged in its igneous composition, other than the gain of H₂O), hydrated and metasomatized, etc.) (2) Metasomatized oceanic igneous rocks were explored using a range of volcanic rock compositions and a troctolite. (3) The effects of strong Ca-Al metasomatism were assessed using a rock from DSDP Leg 37 and an epidosite from Tonga. (4) depleted mantle was included as an end-member unmetasomatized peridotite. (5) The effects of metasomatism of oceanic mantle were investigated using peridotites from the Shaka and Islas Orcadas fracture zones. (6) Oceanic sediments were modeled with four disparate bulk compositions: chert from the Mariana trench, clay from the Mariana

trench, carbonate from the Guatemala trench, and terrigenous debris from the Antilles trench. (7) Subduction erosion was modeled using MORB for oceanic arcs, and a continental gneiss and schist for continental arcs. (8) Last, continental collisions were modeled using a biotite zone pelite and a granitic gneiss.

[6] All the bulk compositions were simplified to the Na₂O-CaO-K₂O-MgO-FeO ± MnO-Al₂O₃-TiO₂-SiO₂-H₂O-(CO₂) system. The exclusion of some components (e.g., Cr) and the absence of some components from solid solution models (e.g., K₂O in amphibole) means that the calculations only approximate natural rocks and minerals. K₂O poses perhaps the greatest problem of this type in this study because it stabilizes K-white mica, a hydrous phase present at a wide range of pressures and temperatures; neglecting the presence of K₂O in amphibole means that the stability of K-white mica is overemphasized.

[7] The calculated phase diagrams are shown in Figures 1–6; all the subsections shown here are H₂O saturated for the sake of completeness and consistency. Each figure includes general rock names, and each is color coded to show the amount of crystallographically bound H₂O, with purple

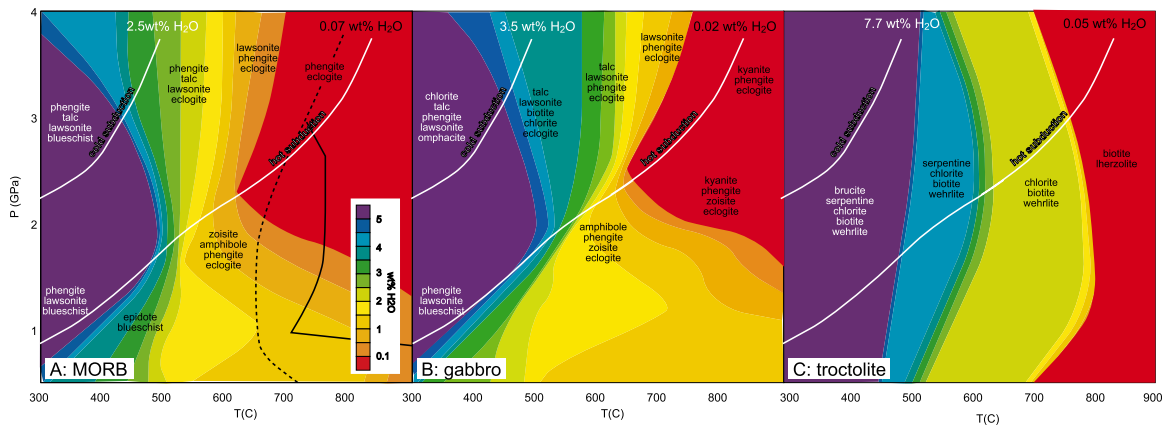


Figure 1. Phase diagrams for unmetasomatized oceanic crust calculated with *Perple_X*: (a) MORB; (b) gabbro [Dick *et al.*, 2000]; and (c) troctolite 209-1275B-6R-1, 61-64 (from IODP hole 1275D [Kelemen *et al.*, 2004]). H₂O-saturated and dehydration solidi for MORB [Vielzeuf and Schmidt, 2001] shown with dashed and solid black lines. MORB and gabbro are similar and subduct 2.5–3.5 wt % H₂O in a cold zone, whereas the high Mg/Si troctolite subducts ~8 wt % H₂O. All three undergo nearly complete dehydration in hot slabs.

indicating >5 wt % H₂O and red <0.1 wt % H₂O (see scale in Figures 1–6). Two schematic subduction *P–T* paths are shown: a cold slab and a hot slab. The two “wt % H₂O” numbers of

each panel indicate the amount of crystallographically bound H₂O reaching postarc depths of 4 GPa along the two end-member *P–T* paths (e.g., in Figure 1a, 2.5 wt % and 0.07 wt % H₂O are

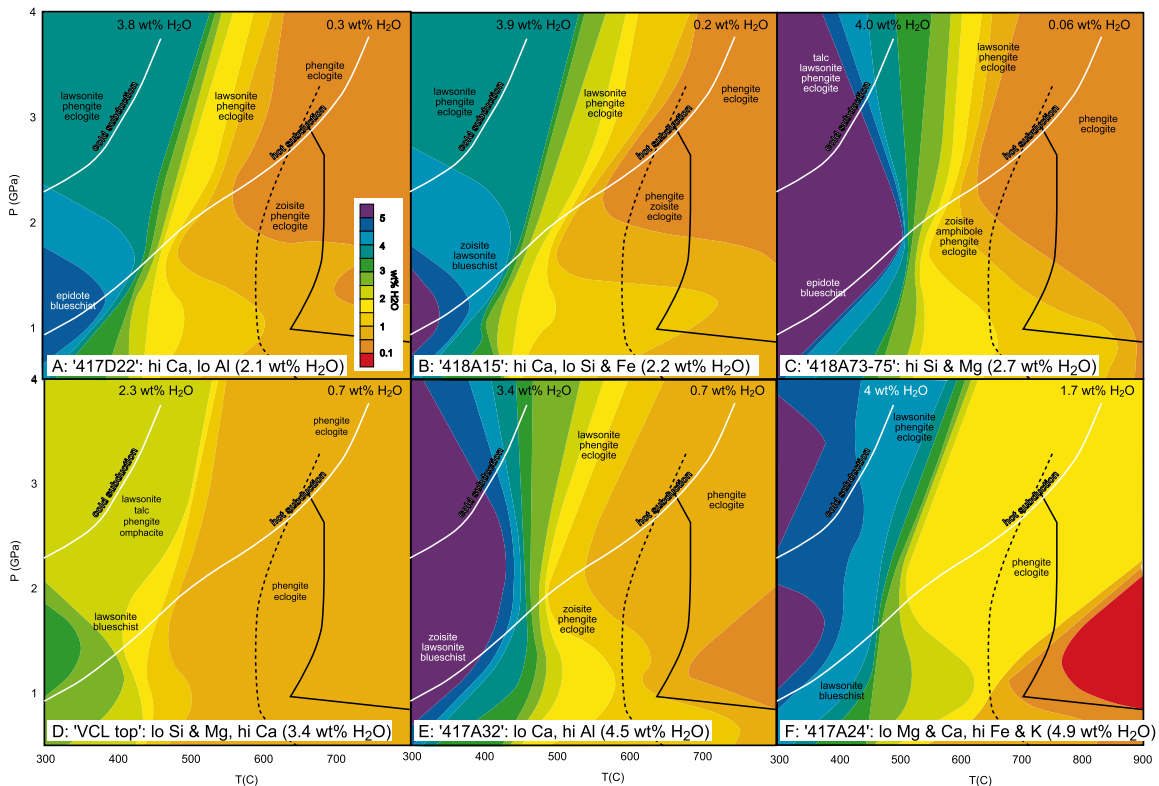


Figure 2. Phase diagrams for metasomatized oceanic volcanic rocks from DSDP holes 417 and 418 [Staudigel *et al.*, 1996] calculated with *Perple_X*; H₂O-saturated and dehydration solidi for MORB [Vielzeuf and Schmidt, 2001] shown with dashed and solid black lines. (a–f) In order of increasing initial H₂O content, shown in parentheses. In cold zones, the postarc slab H₂O scales with initial H₂O because of the stability of lawsonite. In hot zones, H₂O scales with bulk rock K₂O.

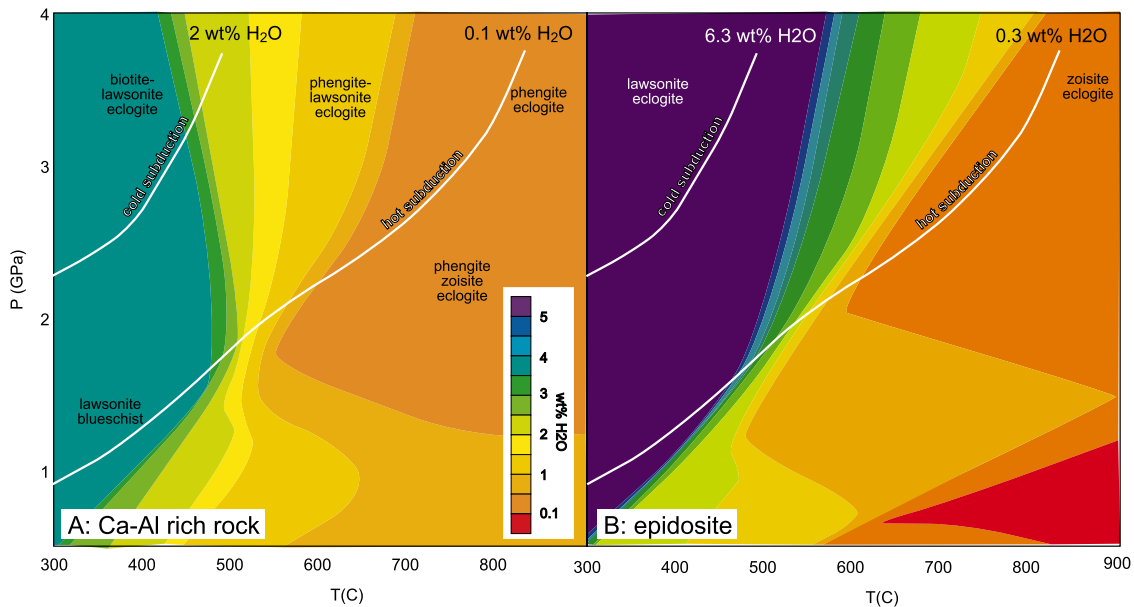


Figure 3. Phase diagrams for oceanic volcanic rocks with strong Ca + Al metasomatism calculated with *Perple_X*. (a) Ca-Al rock DSDP037-0332B-022-003/3-5 [Gunn and Roobol, 1977] and (b) epidosite [Banerjee et al., 2000]. In contrast to typical metasomatized volcanic rocks (Figure 2), epidosites are not able to entrain significant H₂O because of low K₂O.

subducted to postarc depths in the cold and hot slabs shown, respectively).

2.1. Unmetasomatized Igneous Rocks

[8] We begin (Figure 1) by examining the phase relations and H₂O-carrying capacity of unmetasomatized, H₂O-saturated mafic crust, using MORB [Pearce, 1976; Wilson, 1989], the calculated composition of lower crustal gabbro from the southwest Indian Ridge [Dick et al., 2000], and a trocto-

lite from IODP hole 1275B [Kelemen et al., 2004]. Both the MORB and gabbro bulk compositions have similar calculated phase relations (phengite-lawsonite eclogite at low T/high P and phengite ± kyanite eclogite at high T/high P) and lead to the subduction of ~3 wt % H₂O in a cold slab. The much greater Mg/Si ratio of the troctolite, most simply evident in the presence of modal olivine, stabilizes serpentine and brucite at low temperature, leading to the subduction of nearly 8 wt % H₂O in a

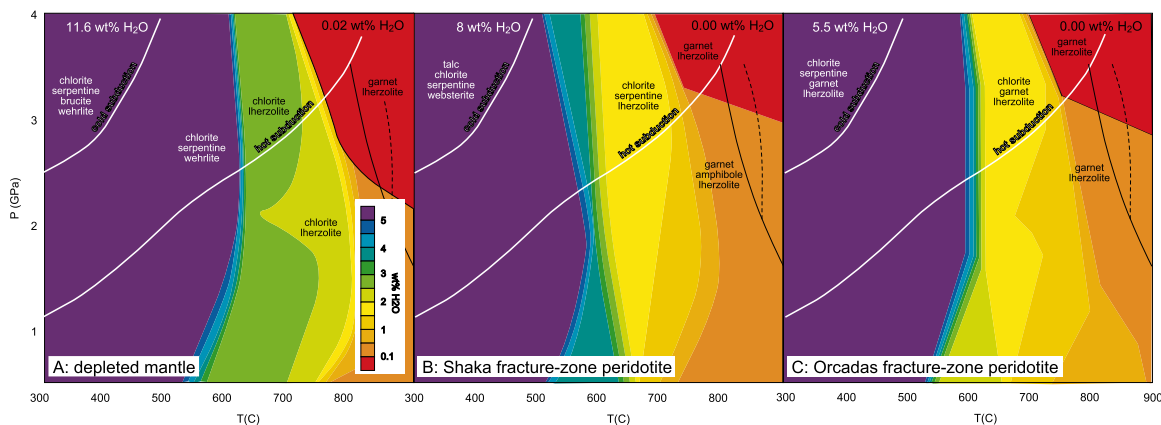


Figure 4. Phase diagrams for oceanic mantle calculated with *Perple_X*; H₂O-saturated and dehydration solidi for depleted mantle [Grove et al., 2006] shown with dashed and solid black lines. (a) DMM (MORB-source depleted mantle) [Workman and Hart, 2005]; (b) Shaka fracture zone peridotite 63-19 [Snow and Dick, 1995]; and (c) Isla Orcadas fracture zone peridotite 58-9B [Snow and Dick, 1995]. In cold slabs the fracture zone peridotites carry less H₂O than depleted mantle. In hot slabs there is no H₂O because of the absence of K₂O.

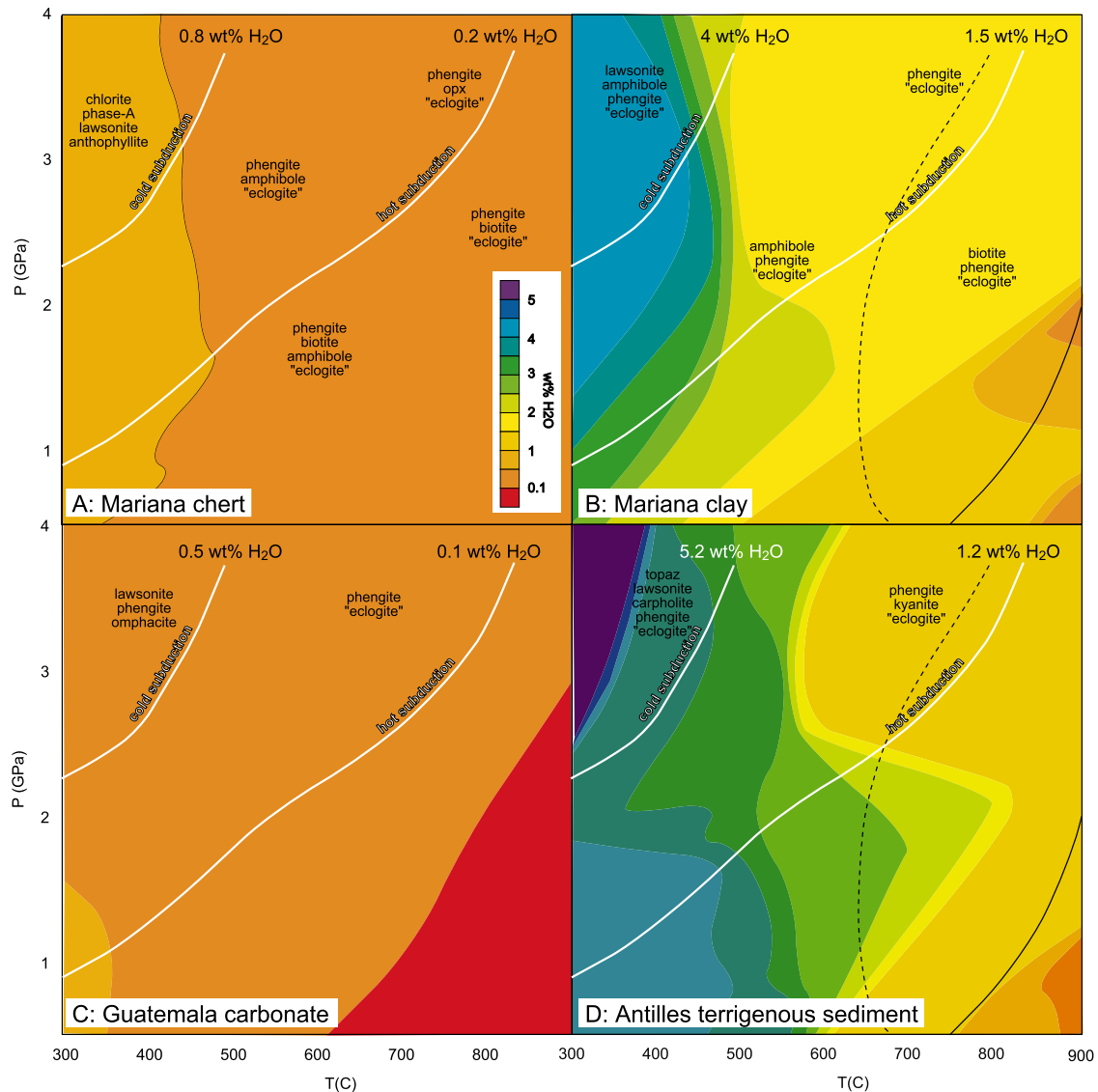


Figure 5. Phase diagrams for oceanic sediments from *Plank and Langmuir* [1998] calculated with *Perple_X*; H₂O-saturated and dehydration solidi for pelite [*Schmidt et al.*, 2004] shown with dashed and solid black lines. Only small volumes of hydrous phases are stable in chert and carbonate, mandating low subducted H₂O contents. The K₂O-rich Antilles and Mariana bulk compositions produce significant postarc slab H₂O flux. “Eclogite” appears in quotes here because these are not true eclogites, but eclogite-facies felsic rocks.

cold slab. All three rock types undergo nearly complete dehydration in hot slabs before temperatures of 600–700°C are reached, because of their miniscule K₂O contents.

[9] The calculated phase diagram for MORB is similar to that constructed by *Schmidt and Poli* [1998] chiefly from experimental data, excepting that it does not include chloritoid, the stability of which in MORB is in doubt [*Hacker et al.*, 2003a]. The upper pressure stability limit for amphibole eclogite is 2.2 GPa, similar to that seen in experiments [*Schmidt and Poli*, 2003]. *Schmidt and Poli*

[1998] inferred that MORB at postarc depths contains 1 (0.5) wt % H₂O in cold (hot) slabs, different than the 2.5 (0.07) wt % calculated here.

2.2. Metasomatized Igneous Rocks

[10] Seafloor metasomatism of oceanic volcanic rocks is typified by the compositions of rocks recovered from DSDP holes 417 and 418 [*Staudigel et al.*, 1996]. These rocks are spilites that show a range of metasomatically induced variations: Si, Al, Fe, Mg, Ca, and K vary from MORB by as much as 46, 57, 34, 55, 140 and 1000%, respec-

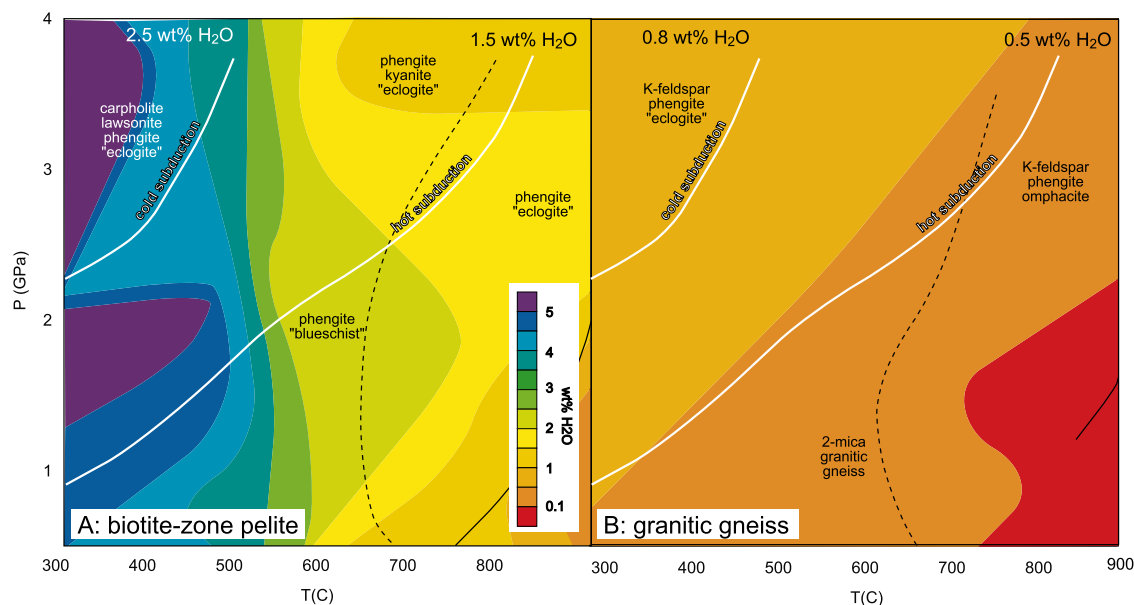


Figure 6. Phase diagrams for continental rocks calculated with *Perple_X*: a biotite zone pelite [Ferry, 1982] and an ultrahigh-pressure gneiss [Johnston, 2006]; H₂O-saturated and dehydration solidi for pelite [Schmidt *et al.*, 2004] and tonalite [Stern *et al.*, 1975; Patiño Douce, 2005] shown with dashed and solid black lines. Modest K₂O contents translate into modest transport of H₂O to postarc depths. “Eclogite” appears in quotes here because these are eclogite-facies felsic rocks.

tively (Table 1). All these bulk compositions have similar calculated mineralogies (lawsonite-phengite ± talc eclogite at low T and phengite eclogite at high T). For cold slabs, the bound H₂O content scales closely with bulk rock Al₂O₃; this behavior is due to the low-temperature stability of the aluminous mineral lawsonite in all these bulk compositions [cf. Rüpke *et al.*, 2004]. In contrast, at high temperature the bound H₂O content scales closely with the bulk rock K₂O content (see below). This behavior arises because the stability of phengite in these rocks is limited only by the availability of K₂O [Schmidt and Poli, 1998]. Kerrick and Connolly [2001b] and Rüpke *et al.* [2004] modeled the *P–T* relations and H₂O content of a fictive composition intermediate between 417A32 and 418A73 (Figure 2), but limited the bulk rock H₂O to 2.5 or 2.7 wt %, resulting in a smaller postarc H₂O flux in cold slabs.

2.3. Epidosites

[11] One of the most extreme forms of metasomatism of the ocean crust is the formation of epidote-rich rocks formed by the leaching of Mg and the deposition of Ca and Al, and one might imagine that such rocks would be major carriers of H₂O to postarc depths. The affect of Ca-Al metasomatism on H₂O subduction is assessed in Figure 3 using two bulk compositions: a Ca-Al rich rock from

DSDP Leg 37 [Gunn and Roobol, 1977] and an epidosite from the Tonga forearc [Banerjee *et al.*, 2000]. The Ca-Al rich rock is similar to the metasomatized volcanic rocks of Figure 2, whereas the epidosite is quite H₂O rich because of its bulk composition is the closest to lawsonite of all the rocks considered. In hot slabs, both of these rocks contrast with metasomatized volcanic rocks in that they are not able to entrain significant H₂O because of their low K₂O content.

2.4. H₂O-Saturated Depleted Mantle and Fracture Zone Peridotites

[12] Fresh oceanic peridotite lacks hydrous phases. However, if H₂O saturated, such rock (“DMM” composition of Workman and Hart [2005]) can contain an enormous proportion of hydrous phases at low T, resulting in subduction of nearly 12 wt % H₂O to 4 GPa (Figure 4a). The presence of only 0.006 wt % K₂O in the “DMM” composition leads, however, to retention of <0.1 wt % H₂O (in phlogopite) to postarc depths in hot slabs. The calculated phase diagram for DMM shows upper thermal stability limits for chlorite and serpentine that are ~100°C colder than those reported from experiments [Schmidt and Poli, 1998], but essentially the same as the hydrous peridotite modeled by Rüpke *et al.* [2004]. To explore the effect that metasomatism has on H₂O retention in oceanic

peridotite, consider peridotites from the Shaka and Islas Orcadas fracture zones (Figures 4b and 4c) [Snow and Dick, 1995]. Both these rocks have more Si and Na, and less Al and Mg than DMM, leading to the stability of talc in the Shaka rock; the absence of brucite in the Orcadas rock, in contrast to DMM, is due to its lower Mg/Si ratio. Because fertile peridotites are capable of hosting even more H₂O than DMM [Schmidt and Poli, 1998], it is perhaps unexpected that both these fracture zone peridotites have generally lower H₂O contents than DMM. As with volcanic rocks, in cold slabs, peridotites undergo little dehydration, such that their bound H₂O content scales with the initial H₂O content. In hot slabs, no H₂O is carried to magma generation depths because peridotites lack the key ingredient K₂O.

2.5. Oceanic Sediment

[13] Oceanic sediments were modeled with four disparate bulk compositions from Plank and Langmuir [1998]: chert from the Mariana trench, clay from the Mariana trench, carbonate from offshore Guatemala, and terrigenous debris from the Antilles (Figure 5). The phase relations of the chert and carbonate do not depend strongly on P and T, as expected for bulk compositions dominated by quartz and calcite/aragonite; consequently, the bound H₂O contents at 4 GPa are small for these rocks in both hot and cold slabs. In contrast, the terrigenous Antilles and clay-rich Mariana bulk compositions stabilize several hydrous phases at low temperature, resulting in significant H₂O flux to 4 GPa in cold slabs. They also contain ~25–30 vol% phengite at high temperature, resulting in subduction of 1.2–1.5 wt % H₂O to postarc depths in hot slabs unless melting occurs.

2.6. Subduction Erosion

[14] Scholl and von Huene [2008] have shown that forearc material in oceanic and continental arcs is being subducted at a global rate of ~1.4 km³/a. Figure 6 shows modeled phase relations for typical continental rocks by using a biotite zone pelite [Ferry, 1982] and a granitic gneiss [Johnston, 2006]. These continental rocks have lower bulk H₂O contents than oceanic clay-rich sediments, reflecting the devolatilization that attends continental metamorphism. All three give off little of their initial H₂O in cold slabs because of the stability of lawsonite and phengite. In hot slabs, it is the stability of phengite that carries the bulk of this

H₂O to postarc depths prior to melting, similar to pelagic sediments.

2.7. Continental Subduction

[15] The subduction of continental crust has generally not been included in discussions of H₂O subduction, but there is a growing recognition that significant volumes of continental material have been subducted. Once-subducted continental margin rocks (“ultrahigh-pressure or UHP” rocks) have been recognized around the world in most Phanerozoic orogens with continental lower plates [Liou et al., 2004]. The densities of such materials suggest that many more UHP terranes were never fully exhumed and may constitute a significant volume of mid–lower crust worldwide [Walsh and Hacker, 2004]. Xenoliths from the Pamir demonstrate that subducted crustal material can attain temperatures of 1100°C where it undergoes extreme processing to make a dehydrated and anhydrous residuum [Hacker et al., 2005]. In the following section, continental subduction is modeled using the lithologies of Figure 6.

2.8. Summary of the H₂O Content of Subducted Rocks

[16] Which bulk compositions, then, are best suited to subducting H₂O to postarc depths? Figure 7 shows H₂O contents for the modeled bulk compositions in hot and cold slabs at 4 GPa. In cold slabs, the rocks best suited to carrying H₂O to postarc depths are troctolite and peridotite, because their high Mg/Si ratios stabilize serpentine, an exceptionally hydrous mineral; carbonate sediment and chert carry the least H₂O. In contrast, in hot slabs, the rocks best suited to carrying H₂O to postarc depths are continental gneisses and schists and clay-rich pelagic sediments (Figure 7), because their high K₂O contents stabilize phengite, which is stable to greater than 4 GPa [Schmidt and Poli, 1998]; melting will remove H₂O and K₂O from the rock, reducing this relationship. A very general, but useful, rule then is that the amount of H₂O subducted to postarc depths in hot slabs is proportional to the K₂O content of the bulk rock composition (Figure 8).

3. Global Postarc Slab H₂O Flux

[17] The implications that these models for various rock compositions have for the global subduction of H₂O to postarc depths can be determined by assessing the relative fluxes of such rocks into subduction zones worldwide (Table 3). To do this,

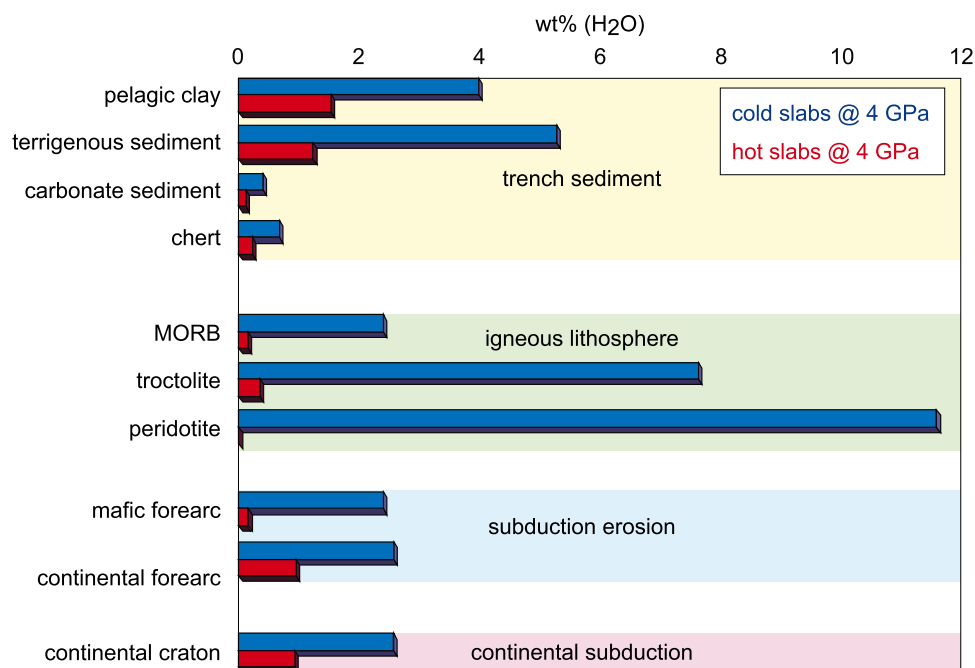


Figure 7. Variability in maximum H₂O content at 4 GPa as a function of rock type in hot and cold slabs. Troctolite and peridotite are best suited to carry H₂O to postarc depths in cold slabs. K-rich continental gneisses and schists and clay-rich pelagic sediments carry the most H₂O in hot slabs.

the subducted materials were divided into the following groups: pelagic sediments, terrigenous sediments, upper volcanic crust, lower volcanic crust, dikes, plutonic rock, mantle, continental gneiss, continents schist, mafic forearc, and continental forearc. Data sources for oceanic subduction zone parameters were: age of subducting plate [Lallemand *et al.*, 2005], length [Jarrard, 2003], plate dip (supplemented by Jarrard [2003], Lallemand *et al.* [2005], and Syracuse and Abers [2006]), subduction erosion rate [Clift and Vannucchi, 2004], and subduction velocity (intermediate value of Jarrard [2003], Lallemand *et al.* [2005], and Syracuse and Abers [2006]), neglecting the eastern Sunda, Aegean, New Zealand, and smaller arcs because of incomplete data sets. This data set encompasses a global ocean floor subduction rate of ~ 2.7 km²/a. Note that the division of the semicontinuous arc systems into arc segments (e.g., splitting South America into Colombia, Peru, N Chile, and S Chile subduction zones), although motivated by real along-strike differences, creates artificial subdivisions in the data set and calculation outcomes.

[18] To calculate the postarc slab H₂O flux for individual subduction zones, the temperature at 4 GPa in the upper 20 km of the slab must be determined for each subduction zone of interest. To do so, thermal models calculated by P. van Keken

(personal communication, 2007) for specific subduction zones were generalized to all subduction zones by using the slab thermal parameter of Kirby *et al.* [1991]:

$$\text{slab thermal parameter (km)} = \frac{\text{plate age}}{\text{slab descent rate}}$$

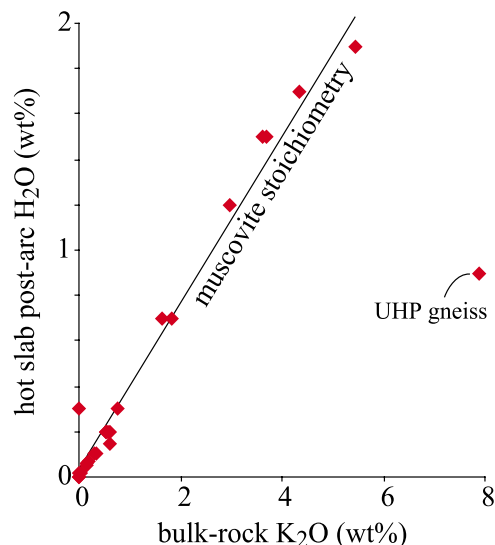


Figure 8. Amount of H₂O subducted to postarc depths in hot slabs scales with bulk rock K₂O.

Table 3. (Representative Sample). Calculated Subarc H₂O Fluxes [The full Table 1 is available in the HTML version of this article at <http://www.g-cubed.org>.]

	Oregon-													
	Lesser Antilles	Sandwich	S Chile	N Chile	Peru	Colombia	Costa Rica	Nicaragua	Guatemala	Mexico	Washington	British Columbia	Alaska	Aleutians
Length, km	850	1005	2000	2000	1599	1355	450	275	500	1383	850	550	1490	1246
Age of oceanic plate, Ma	91	38	34	53	36	15	26	24	18	13	11	8	47	55
Orthogonal convergence rate, km/Ma	18	44	70	79	67	55	72	71	67	52	28	41	55	59
Descent rate, km/Ma	12	40	40	39	14	30	62	63	56	22	7	13	37	48
Sediment thickness, ^a km	3.42	0.208	2.144	0.15	0.378	0.318	0.208	0.156	0.156	0.318	1.386	1.6	1.6	0.885
Sediment bulk composition ^b	terrigr	terrigr	carb	carb	carb	carb	carb	carb	carb	pel	pel	pel	terrigr	pel
Subarc H ₂ O, wt %	1.20	1.20	0.12	0.12	0.12	0.12	0.12	0.12	0.12	1.60	1.60	1.60	1.20	1.60
Pelagic sediment	1.20	1.20	1.20	1.20	1.20	1.20	1.20	1.20	1.20	1.20	1.20	1.20	1.20	1.20
Terrigenous sediment	0.19	0.19	0.19	0.19	0.19	0.19	0.19	0.19	0.19	0.19	0.19	0.19	0.19	0.19
Upper volcanic rock	0.08	0.08	0.08	0.08	0.08	0.08	0.08	0.08	0.08	0.08	0.08	0.08	0.08	0.08
Lower volcanic rock	0.08	0.08	0.08	0.08	0.08	0.08	0.08	0.08	0.08	0.08	0.08	0.08	0.08	0.08
Dikes	0.79	0.79	0.79	0.79	0.79	0.79	0.79	0.79	0.79	0.05	0.05	0.05	0.79	0.79
Gabbro	2.0	2.0	2.0	2.0	2.0	1.9	2.0	2.0	2.0	0.0	0.0	0.0	2.0	2.0
Mantle														
Continental rock														
Mafic forearc	0.1	0.1	0.1	0.1	0.1	0.1	0.1	0.1	0.1	0.1	0.1	0.1	0.1	0.1
Continental forearc	1.2	1.0	1.0	1.0	1.0	1.0	1.0	1.0	1.0	1.0	1.0	1.0	1.0	1.0
Subarc H ₂ O flux, Tg/Ma														
Pelagic sediment	1.8.E+05	2.9.E+05	1.5.E+05	7.5.E+04	9.2.E+04	6.3.E+04	2.1.E+04	9.7.E+03	1.7.E+04	8.1.E+05	3.2.E+05	3.1.E+05	8.3.E+05	9.2.E+05
Terrigenous sediment	9.5.E+05	7.6.E+06	3.7.E+05	1.3.E+05	3.7.E+05	1.3.E+05	1.2.E+05	5.4.E+05	5.6.E+04	1.2.E+05	5.4.E+05	7.4.E+05	2.5.E+06	1.2.E+06
Upper volcanic rock	2.5.E+04	7.3.E+04	2.3.E+05	2.6.E+05	1.8.E+05	1.2.E+05	5.4.E+04	3.3.E+04	5.6.E+04	1.2.E+05	4.0.E+04	3.8.E+04	1.4.E+05	1.2.E+05
Lower volcanic rock	1.1.E+04	3.1.E+04	1.0.E+05	1.1.E+05	7.6.E+04	5.3.E+04	2.3.E+04	1.4.E+04	2.4.E+04	5.1.E+04	1.7.E+04	1.6.E+04	5.8.E+04	5.2.E+04
Dikes	5.1.E+04	1.5.E+05	4.7.E+05	5.3.E+05	3.6.E+05	2.5.E+05	1.1.E+05	6.5.E+04	1.1.E+05	2.4.E+05	7.9.E+04	7.5.E+04	2.7.E+05	2.5.E+05
Gabbro	1.8.E+06	5.2.E+06	1.7.E+07	1.9.E+07	8.0.E+05	5.6.E+05	3.8.E+06	2.3.E+06	4.0.E+06	5.4.E+05	1.8.E+05	1.7.E+05	9.7.E+06	8.7.E+06
Mantle	3.7.E+06	1.1.E+07	3.4.E+07	3.8.E+07	2.6.E+07	1.7.E+07	7.8.E+06	4.7.E+06	8.0.E+06				2.0.E+07	1.8.E+07
Continental rock														
Mafic forearc														
Continental forearc		2.3.E+05												
Subduction erosion		2.3.E+05												
Total	6.7.E+06	1.7.E+07	5.9.E+07	6.5.E+07	3.3.E+07	2.2.E+07	1.3.E+07	7.6.E+06	1.3.E+06	4.8.E+05	1.4.E+06	1.3.E+06	3.3.E+07	2.9.E+07

^a Clift and Yánucci [2004].

^b Lallemand et al. [2005].

^c 67% pelagic + 33% carbonate.

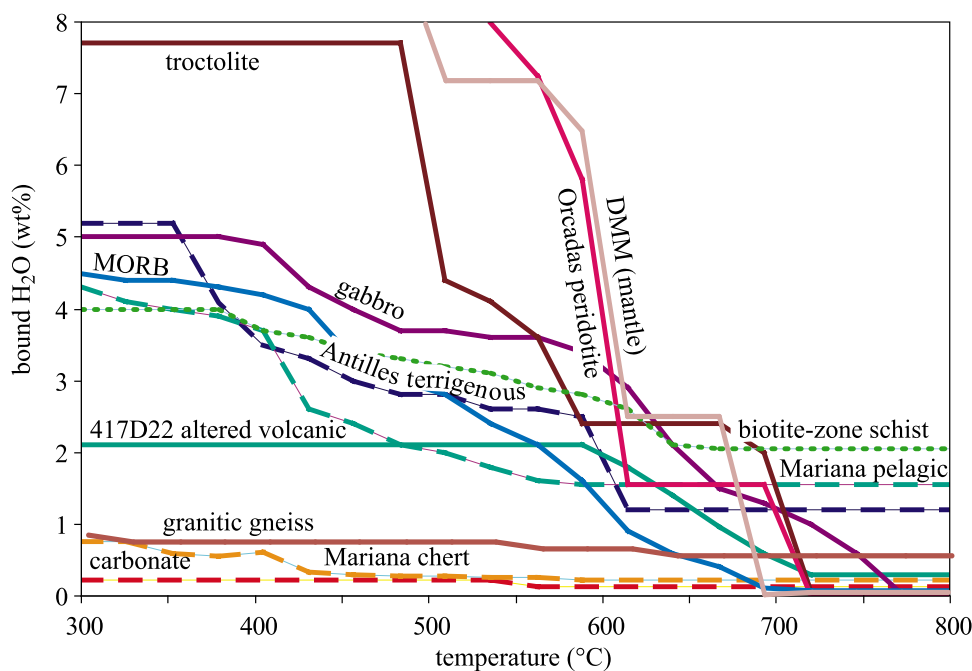


Figure 9. Calculated bound H₂O content at 4 GPa as a function of temperature.

This gave a fit of

$$T^{\circ}C(\text{at } 4 \text{ GPa}) = 894 - 21 \ln(\text{thermal parameter})$$

for the top of the slab,

$$T^{\circ}C(\text{at } 4 \text{ GPa}) = 1378 - 114 \ln(\text{thermal parameter})$$

for the slab Moho, and

$$T^{\circ}C(\text{at } 4 \text{ GPa}) = 1387 - 108 \ln(\text{thermal parameter})$$

for 20 km deep within the slab. Temperatures for intermediate levels within a slab at 4 GPa were interpolated linearly.

[19] The Perple_X-specified H₂O content of each rock type at 4 GPa (Figure 9) was approximated with two-part linear models. For example, for the gabbro of Figure 1, the calculated H₂O content was approximated as:

$$H_2O(\text{wt } \%) = 9.7 - 0.01 * T^{\circ}C; \quad T < 750^{\circ}C$$

$$H_2O(\text{wt } \%) = 0.03; \quad T \geq 750^{\circ}C$$

The postarc flux of H₂O for each rock type in each subduction zone was then determined from this H₂O content, the orthogonal subduction rate,

thickness of the rock type of interest, and the trench length:

$$H_2O \text{ mass flux} = H_2O \text{ wt } \% * \text{subduction rate}$$

$$* \text{rock thickness} * \text{density} * \text{trench length}$$

3.1. Sediment

[20] Pelagic sediment thicknesses and compositions were taken from *Plank and Langmuir [1998]* and *Plank et al. [2007]* (Table 3); the composition of sediment subducted at each trench was simplified to one of the four types in Figure 5: clay-rich pelagic, terrigenous, chert, or carbonate (exception: the compositions of the Mariana sediments lie far enough from these end-members that they were modeled using the actual compositions, and Philippine Trench sediments lie far enough that they were modeled as binary mixtures of clay-rich and chert or carbonate sediments). Pelagic sediment thicknesses are 200–500 m in many subduction zones; exceptions are the Antilles, Cascadia, Alaska, Sumatra, Andaman, and Makran arcs, and, to a lesser extent, the IBM and Solomon arcs; four trenches are subducting the juiciest pelagic sediments: Kurile, NE Japan, Tonga, and Kermadec, whereas the trenches from Guatemala to Chile are

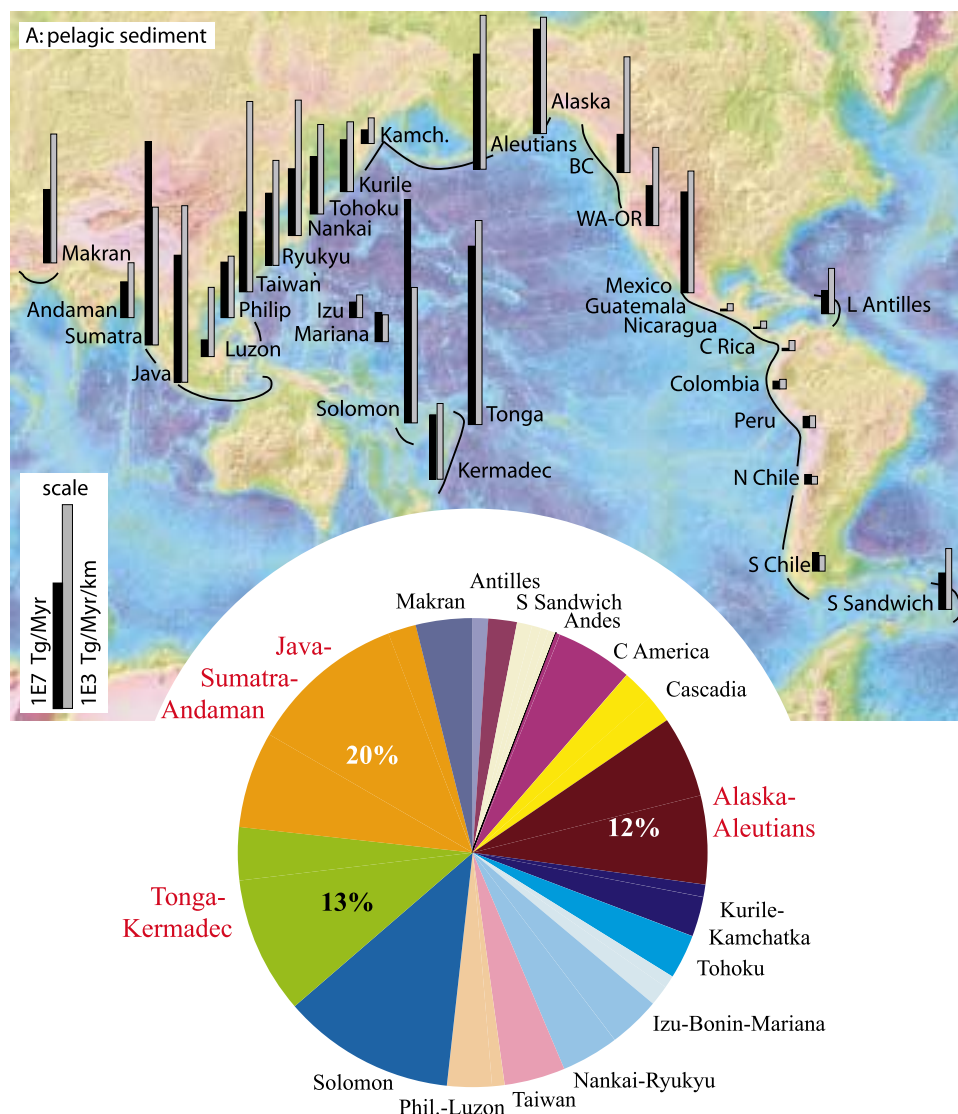


Figure 10. Fluxes of H₂O delivery (black bars, Tg/Ma, and pie diagram) and per-km rates of H₂O delivery (gray bars, Tg/Ma/km) to postarc depths from (a) pelagic sediment, (b) terrigenous sediment, (c) igneous oceanic lithosphere, (d) subduction erosion, and (e) all sources. Topography from *Smith and Sandwell* [1997].

subducting dry carbonate. Trench sediment thicknesses were taken from *Clift and Vannucchi* [2004]; they tend to scale with pelagic sediment thickness, except in S Chile and Taiwan, which have >3 km of trench sediment in spite of minor pelagic sediment input. For the purpose of this study, trench sediment <500 m thick was assumed to be of the pelagic composition specified by *Plank and Langmuir* [1998], whereas trench sediment in excess of 500 m was assumed to be terrigenous (and modeled as “Antilles terrigenous”).

[21] The fraction of the trench sediment subducted to postarc depths was taken from *Clift and Vannucchi* [2004]: at erosive margins all trench sedi-

ment is being subducted, whereas at accretionary margins only a fraction is being subducted. The rate at which pelagic sediments are being subducted shows minor variation globally, from ~10–20 km³/Ma/km, but the variation in the rate at which H₂O is being delivered to postarc depths (Tg/Ma/km) is considerably greater because of the variation in slab temperature and sediment composition: the three most important subduction zones are Tonga, Solomons and Java. When this value is combined with subduction zone length to yield the postarc slab H₂O flux for each arc (Tg/Ma) (Figure 10a), the Java-Sumatra-Andaman arc reigns supreme, but the Tonga-Kermadec and Alaska-Aleutian arcs are also significant. A few arcs,

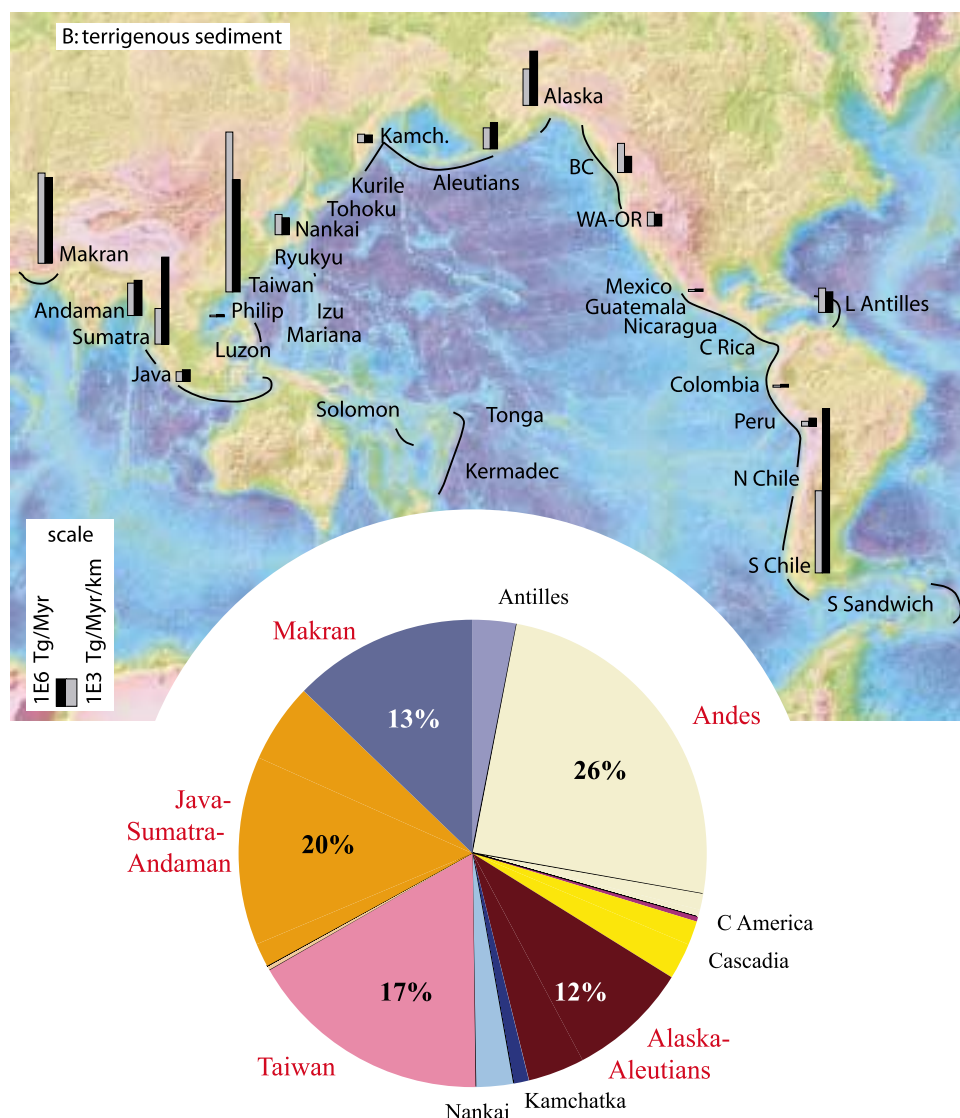


Figure 10. (continued)

chiefly in Central and South America, have essentially zero H₂O flux from pelagic sediments.

[22] The terrigenous sediment subduction rate varies globally enormously from 0 to 160 km³/Ma/km and is utterly different than that for pelagic sediments. The variation in the rate (Tg/Ma/km) at which H₂O is being delivered to postarc depths by terrigenous sediment is even more extreme than for pelagic sediment: the three dominant subduction zones are S Chile, Taiwan, and the Makran. When this value is combined with subduction zone length to yield a postarc slab H₂O flux (Tg/Ma) for terrigenous sediment, five subduction zones carry the bulk of terrigenous sediment hosted H₂O to 4 GPa: Andes, Alaska-Aleutians, Taiwan, Java-Sumatra, Andaman, and Makran (Figure 10b).

[23] *Kerrick and Connolly* [2001a] modeled the phase relations of four other sediment compositions: global average subducted sediment (GLOSS), an Fe-calcite clay from the Antilles, a cherty limestone from Mariana, and a nannofossil ooze from Vanuatu. Their cherty limestone is similar in composition to a mixture of our Mariana chert and Guatemala carbonate and yields low postarc slab H₂O fluxes. Our pelagic and terrigenous sediments have similar calculated H₂O fluxes to their nannofossil ooze and calcite clay. GLOSS appears to be the most efficient carrier of H₂O to postarc depths [see also *Rüpke et al.*, 2004], but recall that this is a fictive global average sediment and not an actual rock.

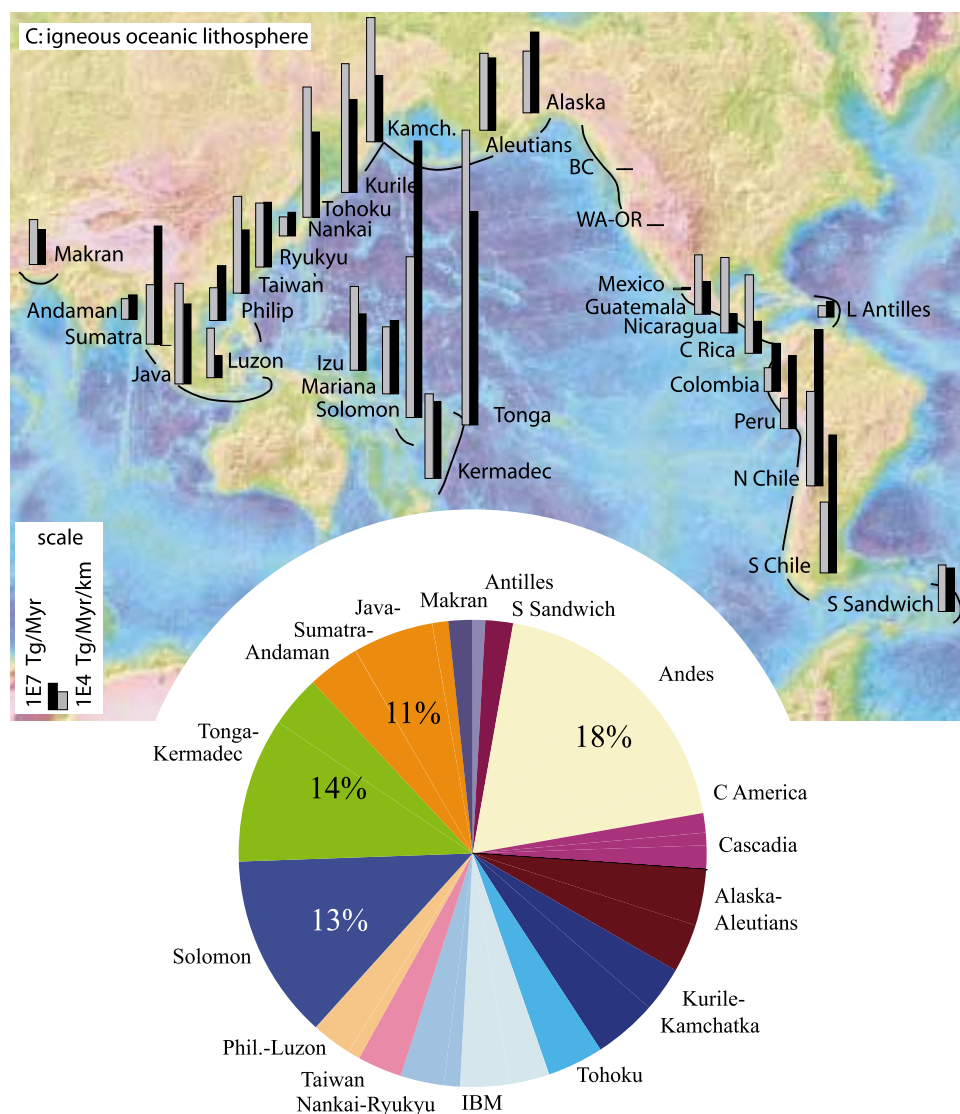


Figure 10. (continued)

3.2. Oceanic Lithosphere

[24] Our understanding of oceanic lithosphere hydration is rudimentary. ODP drill cores show that much hydration occurs near the ridge axis, and that hydration continues as the lithosphere ages [Jarard, 2003]. Considerable additional hydration may occur during deformation at outer arc rises. Quantification of possible outer arc-rise hydration has been attempted from analysis of seismic wave speeds: Contreras-Reyes *et al.* [2007] showed that P wave velocities decrease from 4.2 to 3.7 km/s in the upper crust and from 7.0–7.1 to 6.9 km/s in the lower crust across the outer rise offshore southern Chile, and Ranero and Sallares [2004] noted similar velocity decreases offshore Costa Rica. Attempts to model a 0.1–0.2 km/s velocity de-

crease in gabbro solely as the result of subgreenschist-facies alteration, using Hacker and Abers [2004], however, does not result in a meaningful constraint on the H₂O content because of the large number of potential alteration phases and poorly determined elasticities for some hydrous phases. Better constraints may be derived from the velocity dispersion of waves that travel up slabs from intermediate-depth earthquakes [Abers, 2005]; these studies indicate that the crust of most subducted slabs imaged in this way is 1–13% slower than its surroundings to depths of 150 km. If such slow velocities are interpreted to reflect the degree of alteration of the slab, they may indicate H₂O contents of 1–5 wt % [Abers, 2005]; these may be maxima because fluid may be coming from deeper in the slab and lodging at these levels. From

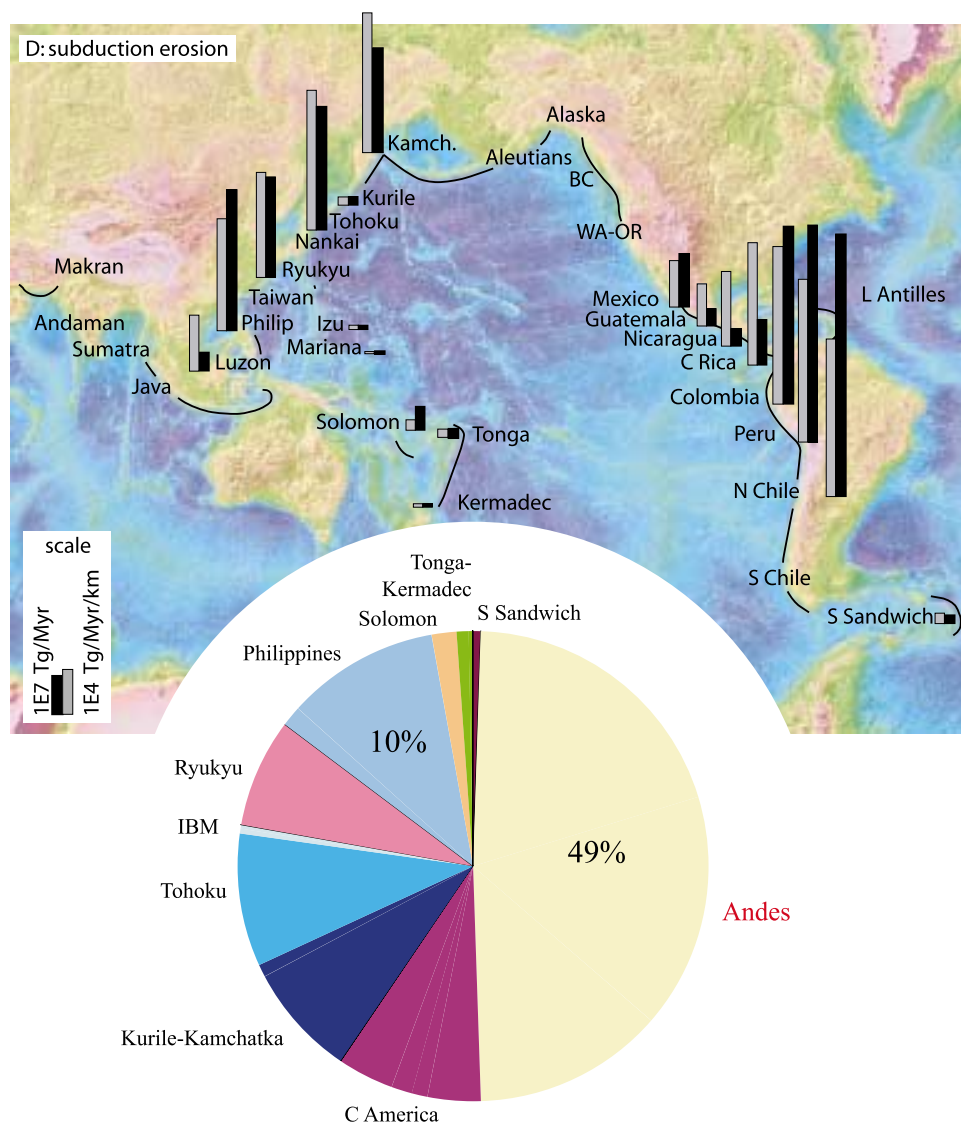


Figure 10. (continued)

measured wave speeds and alteration mineralogies, *Carlson* [2003] estimated that average oceanic lower crust contains 0.5 wt % H₂O.

[25] I use the igneous ocean crust alteration model of *Jarrard* [2003] (Table 3), which calculates the amount of presubduction H₂O and K₂O in oceanic igneous rocks as a logarithmic function of plate age. It assumes 0.3 km of upper volcanics, 0.3 km of lower volcanics, 1.4 km of dikes, and 5 km of gabbro. To convert Jarrard's bound H₂O contents and K₂O contents to postarc slab H₂O fluxes, I determine H₂O at postarc depth in each of the volcanic and dike layers for the bulk composition MORB with the H₂O and K₂O contents specified by the Jarrard model (similar to Figure 1a, which is for a fixed intermediate K₂O content of 0.2 wt %);

I use the gabbro of Figure 1b and the H₂O content specified by the Jarrard model for the gabbroic layer.

[26] Modeling hydration of oceanic mantle is much more problematic because, as emphasized by many authors [e.g., *Wallmann*, 2001; *Poli and Schmidt*, 2002; *Schmidt and Poli*, 2003; *Rüpke et al.*, 2004], rather little is known about such processes in Earth. At fast spreading ridges, the high heat flow keeps the mantle anhydrous [e.g., *Ranero et al.*, 1997], and limited tectonic extension exposes almost no peridotite at the seafloor (J. Karson, personal communication, 2006); slow-spreading ridges undergo more significant hydration and metasomatism [*Canales et al.*, 2000] because of the tighter spacing of spreading-ridge offsets and amagmatic

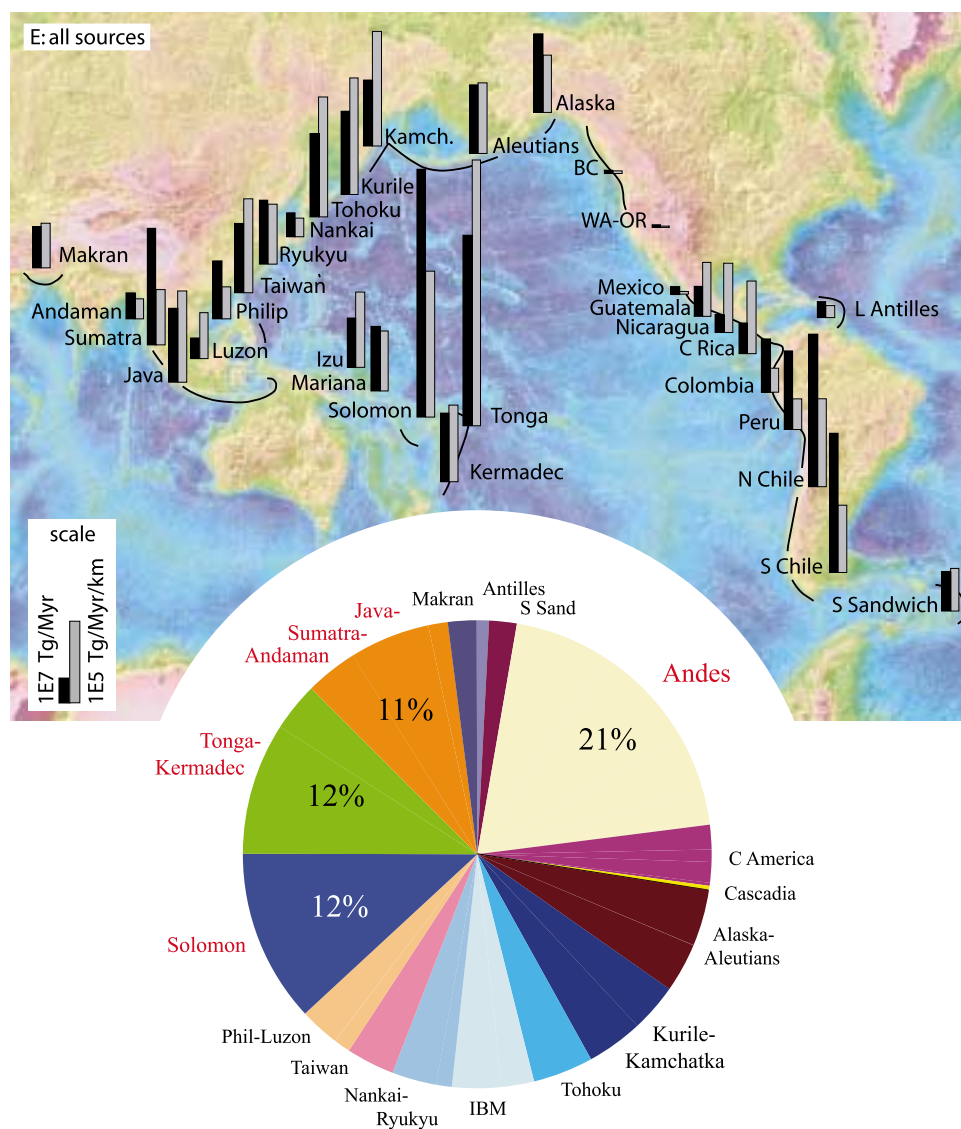


Figure 10. (continued)

extension that exposes peridotite at or near the seafloor [Karson, 1998]. The amount of H₂O that these features lock into oceanic mantle is unknown; Schmidt and Poli [1998], for example, assumed that these processes produced on average 10% serpentine to a depth of 5 km. In recent years, there has been a growing suspicion that most hydration of the oceanic mantle occurs in outer-arc rises where deep faulting and bending permit fluid percolation [Seno and Yamanaka, 1996; Peacock, 2001; Ranero et al., 2005]. Three studies used seismic wave speeds and gravity data to estimate hydration of the oceanic mantle at outer rises: Ranero and Sallares [2004] reported a decrease in V_P to 7.6 km/s in the uppermost 1 km of the mantle subducting beneath northern Chile, Grevemeyer et al. [2007] measured 7.4 km/s in

the uppermost mantle and 7.5–7.8 km/s 3–4 km deeper offshore Costa Rica, and Contreras-Reyes et al. [2007] reported a decrease in V_P to 7.8 km/s in the uppermost 2–2.5 km of the mantle of southern Chile. Modeling these velocity decreases solely as the result of serpentinization, using Hacker and Abers [2004] indicates H₂O contents of 1.8–2.5 wt % (N Chile), 3.1 and 1.8 wt % H₂O (Costa Rica) and 2.0 wt % (S Chile). Ranero and Sallares [2004] used a gravity model to estimate that the depth of serpentinization might reach 20 km into the mantle. On the basis of these observations, for this study, oceanic mantle was modeled as 4 km of hydrous mantle (using the Islas Orcadas peridotite; Figure 4c) with a maximum of 2 wt % H₂O.

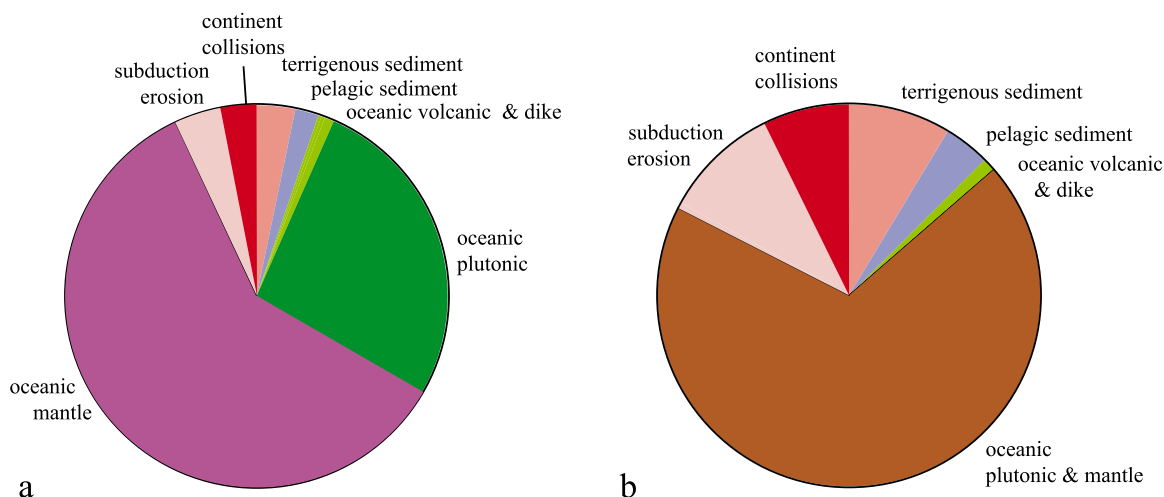


Figure 11. Contributions of subduction processes and rock types to global postarc slab H₂O flux. (a) Oceanic mantle dominates the postarc H₂O flux; contributions from sediment subduction, subduction erosion, and continental collisions are minor. (b) If Wallmann's [2001] estimate of the amount of H₂O subducted to postarc depths in peridotite is correct, the relative contributions of sources such as sediment subduction, subduction erosion, and continental collisions are more significant.

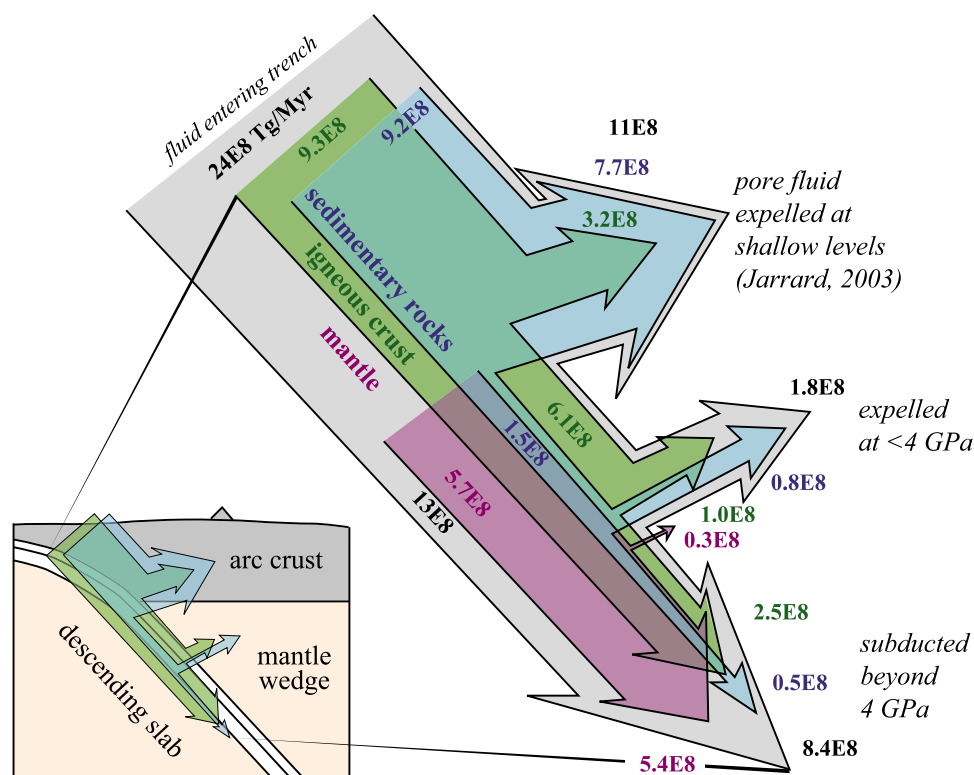


Figure 12. Simplified global H₂O flux from trench to postarc depths for oceanic lithosphere (subduction erosion and continental subduction not shown). See Table 4 for additional information. Widths of arrows are scaled to flux magnitudes, which are given in Tg/Ma. Of the H₂O subducted at trenches in oceanic lithosphere (24E8 Tg/Ma), 46% is driven off by the closure of pores (11E8 Tg/Ma), another 19% (4.6E8 Tg/Ma) is driven off by devolatilization at pressures <4 GPa, and 35% (8.4E8 Tg/Ma) reaches postarc depths.

Table 4. Comparison of Calculated Subduction Zone H₂O Fluxes^a

	P90	B95	W01	J03	SP03	R04	This Study	Combined Studies
Total H ₂ O entering trench								
Sediment				8.9				9.2 ^b
Igneous crust				9.2				9.3 ^b
Mantle								5.7 ^b
Total				18				24 ^b
Pore H ₂ O entering trench								
Sediment				7.7				
Igneous crust				3.2				
Mantle								
Total				11				
Bound H ₂ O entering trench								
Sediment	0.7	0.3–1.4		1.2		1.6	1.5	
Igneous crust	8	9–18	7	6	13–16	4.6	6.1	
Mantle					4.9–8.6	2.4–12	5.7	
Total	8.7	9.3–19.4			18–25	9–18	13	
Subduction erosion							2.2	
Continental collisions							0.51	
Subducted beyond 4 GPa								
Sediment						0.5–0.6	0.5	0.5
Upper volcanic rocks							0.04	0.04
Lower volcanic rocks							0.02	0.02
Dike rocks							0.08	0.08
Plutonic rocks							2.4	
Igneous crust			<2.5 ^c			3.5–3.9	2.5	<2.5 ^d
Mantle			<2.5 ^c			2.4–12	5.4	
Total					4.3–12	6.4–16		<3.1 ^d
Subduction erosion							0.35	0.35
Continental collisions							0.26	0.26
Total							11.6	<3.7 ^d

^aUnits are 1E8 Tg/Ma. P90, *Peacock* [1990]; B95, *Bebout* [1995]; W01, *Wallmann* [2001]; J03, *Jarrard* [2003]; SP03, *Schmidt and Poli* [2003]; R04, *Rüpkke et al.* [2004].

^bComputed using pore fluid estimates of *Jarrard* [2003].

^cFor mantle and crust (except upper 500 m).

^d<2.5E8 Tg/Ma for plutonics rocks + igneous crust + mantle; computed using *Wallmann's* constraint on subduction of H₂O in lower crust and mantle.

[27] The rate (Tg/Ma/km) at which H₂O is being delivered to postarc depths by igneous lithosphere is dominated by the Tonga arc (Figure 10c). When this value is combined with subduction zone length to yield a postarc slab H₂O flux (Tg/Ma), the situation is less lopsided, with the Andes, Tonga-Kermadec, Solomon, and Java-Sumatra-Andaman arcs playing important roles.

3.3. Subduction Erosion

[28] Subduction erosion was modeled using the data of *Clift and Vannucchi* [2004]. Because subducted forearc material is likely to be quite hydrated because of its long-term position above the subducting slab, I assumed that the average oceanic forearc undergoing erosion is completely hydrated MORB and that the average continental forearc

being eroded is an average of completely hydrated sediment and completely hydrated gneiss (using the schist and gneiss in Figures 6b and 6c). This material was assumed to follow the *P–T* trajectory of the slab interface; this results in a dramatic difference between the subduction of volcanic forearc (modeled with low-K MORB that dehydrates almost completely by 700°C) and continental forearc (modeled with potassic schist and gneiss that retain significant H₂O to >700°C). The postarc slab H₂O flux calculated with these assumptions is dominated by the Andean arc (Figure 10d).

3.4. Continental Subduction

[29] Calculating the amount of H₂O subducted to postarc depths in continental collision zones is fraught with uncertainty. We know from ultra-

high-pressure terranes [Chopin, 2003], crustal xenoliths erupted from mantle depths [Hacker *et al.*, 2005], and seismicity in active orogens [Searle *et al.*, 2001] that continental crust is subducted to postarc depths. We do not know the flux of such material. More than twenty ultrahigh-pressure terranes have been exhumed since 500 Ma [Liou *et al.*, 2004]; if we assume that each was once as large as the best known Norwegian and eastern China examples (roughly $10,000 \text{ km}^2 \times 10 \text{ km}$ [Hacker *et al.*, 2000; Hacker, 2007]), this yields a flux of $200 \text{ km}^3/\text{Ma}$. This value is a minimum because of incomplete exhumation; the real flux might be more like $>1000 \text{ km}^3/\text{Ma}$.

[30] Subducting continental crust may be detectable using geophysical methods. Burtman and Molnar [1993] argued that continental crust 20–25 km thick has reached depths of 200 km along a 300-km segment of the Hindu Kush since 15 Ma; this is a flux of continental material to depths $>100 \text{ km}$ of $45\text{E}3 \text{ km}^3/\text{Ma}$. Continental crust that is undetectable using current geophysical methods is likely being subducted in other continent convergence belts. As a crude estimate of continental subduction rates, I assume that in the Alps, Zagros, Tibet, and New Guinea collision zones that a 2-km-thick continental crustal layer is being subducted to postarc depths along the entire length of the subduction zone. Convergence rates for these orogens were taken from Johnson [2002], Tesauero *et al.* [2005], Reilinger *et al.* [2006], and DeMets *et al.* [1994]. I assume that the continental material being subducted is an average of completely hydrated sediment and completely hydrated gneiss (schist and gneiss compositions in Figures 6b and 6c). This material was assumed to follow the P – T trajectory of the slab Moho, approximating half the thickness of a continental margin.

3.5. Summary: Global Postarc Slab H₂O Flux

[31] Combining the various sources of postarc slab H₂O yields the total postarc slab H₂O flux. The grey bars in Figure 10e show the flux for each subduction zone per kilometer, and the black bars show the flux for the entire subduction zone. The arc with the greatest per-km postarc slab H₂O subduction is the Tonga arc, but half a dozen other western Pacific arcs are also large contributors, in large part because these are sites of rapid subduction of old lithosphere. The global postarc slab H₂O flux is dominated by the Andes, but there are half a dozen arc systems playing a major role.

[32] Combining the data for all subduction zones yields a global postarc slab H₂O flux of $9\text{E}8 \text{ Tg}/\text{Ma}$. Figure 11 illustrates the relative roles of different types of rock in delivering postarc slab H₂O. Hydrous peridotite is considered to deliver the greatest postarc slab H₂O flux (60%) [cf. Schmidt and Poli, 1998; Rüpke *et al.*, 2004], whereas hydrous plutonic rocks deliver 28% and sediment subduction 5%. This lopsided difference depends chiefly on the fact that the peridotite and gabbro experience colder P – T paths during subduction compared to all other rocks that are closer to the subduction interface; it has little to do with the initial H₂O contents of the rocks or their capacity to retain H₂O to high pressure.

4. Discussion

4.1. A More Holistic View of H₂O Cycling in Subduction Zones

[33] The present study builds on the foundation of other attempts to constrain H₂O cycling in subduction zones (Figure 12 and Table 4). Early estimates by Peacock [1990] for bound H₂O in subducting sediment and igneous crust were $0.7\text{E}8 \text{ Tg}/\text{Ma}$ and $8\text{E}8 \text{ Tg}/\text{Ma}$. Bebout [1995] used bulk rock analyses of high-pressure metasedimentary rocks to calculate a bound H₂O flux of $0.3\text{E}8$ – $1.4\text{E}8 \text{ Tg}/\text{Ma}$ for sediment and $9\text{E}8$ – $18\text{E}8 \text{ Tg}/\text{Ma}$ for igneous crust.

[34] Wallmann [2001] used the degree of hydration observed in DSDP cores to estimate the flux of bound H₂O in the igneous oceanic crust as $7\text{E}8 \text{ Tg}/\text{Ma}$. Combined with H₂O subduction fluxes from Plank and Langmuir [1998] and Schmidt and Poli [1998], and the ¹⁸O record from marine carbonates, Wallmann concluded that the amount of bound H₂O subducted to postarc depths in oceanic lithosphere, excluding sediments and the upper 500 m of volcanic rocks, is $<2.5\text{E}8 \text{ Tg}/\text{Ma}$.

[35] In an update of their earlier model [Schmidt and Poli, 1998], Schmidt and Poli [2003] assumed that subducted slabs consist of 2 km of H₂O-saturated basalt, 5 km of 20% hydrated gabbro and 5 km of 10–20% serpentinized mantle, to estimate subducted bound H₂O contents of $13\text{E}8$ – $16\text{E}8 \text{ Tg}/\text{Ma}$ and $4.9\text{E}8$ – $8.6\text{E}8 \text{ Tg}/\text{Ma}$ for the igneous crust and mantle, respectively. Using experimentally derived phase diagrams they suggested that between 21 and 52% of this H₂O ($4.3\text{E}8$ – $12\text{E}8 \text{ Tg}/\text{Ma}$) is retained in the slab to depths of 150 km.

[36] *Jarrard* [2003] used an age-based alteration model (see above) to improve the estimate of H₂O bound in igneous crust, and increased the *Plank and Langmuir* [1998] sediment H₂O values by a third to account for the *von Huene and Scholl* [1991] database. He calculated a global flux for pore H₂O and bound H₂O in ocean crust of 18E8 Tg/Ma, contributed subequally from igneous and sedimentary rocks; of this, ~11E8 Tg/Ma was considered to be pore water. H₂O bound in crystals was reported as 6.1E8 Tg/Ma in the igneous crust and 1.2E8 Tg/Ma in subducted sediment.

[37] *Rüpke et al.* [2004, 2006] assumed subduction of 0.35 km or 0.5 km of sediment with 7.3 wt % H₂O, 1 km of volcanic rock with 2.7 wt % H₂O, 2 km of gabbro with 1 wt % H₂O, and 10 km of mantle with up to 5% serpentine (depending on plate age), estimating subduction of 9–18E8 Tg/Ma. They concluded that ~77–89% of that H₂O is subducted to postarc depths.

[38] There are several differences between these studies and the present work (including the subduction database used, the subduction processes considered, and the rock types considered), but useful comparisons can be made. The fluxes for H₂O at 4 GPa calculated in the present study fall within the bounds defined by *Rüpke et al.* [2004], except for the H₂O flux in igneous crust, which is ~1/3 smaller. Adding the pore fluid estimates of *Jarrard* [2003] to the estimates from this paper indicates a total H₂O subduction (in minerals and pores) of 24E8 Tg/Ma, 50% greater than that estimated by *Jarrard*, due almost exclusively to the consideration of hydrated mantle in the present model. Thus, of the H₂O subducted at trenches in oceanic lithosphere (24E8 Tg/Ma), 46% is driven off by the closure of pores (11E8 Tg/Ma), another 19% (4.6E8 Tg/Ma) is driven off by devolatilization at pressures < 4 GPa, and 35% (8.4E8 Tg/Ma) reaches postarc depths. For comparison, arc magmas have been estimated to liberate 1E8–6E8 Tg/Ma [*Ito et al.*, 1983; *Peacock*, 1990; *Wallmann*, 2001; *Hilton et al.*, 2002; *Jarrard*, 2003], equivalent to this estimate of forearc devolatilization. Subduction erosion and continental subduction, not considered in previous models, contribute another 0.6E8 Tg/Ma postarc slab H₂O flux in the present model.

[39] All studies that have considered subduction of hydrated mantle conclude that this dominates postarc H₂O flux (e.g., Figure 11a). If *Wallmann's* [2001] determination of <2.5E8 Tg/Ma postarc subduction of H₂O in the lower crust and upper

most mantle is correct, however, the relative contributions of all other sources are commensurately greater (Table 4 and Figure 11b).

4.2. Implications for Slab Seismicity

[40] If subduction zone seismicity is linked to dehydration reactions in downgoing slabs [e.g., *Kirby et al.*, 1996; *Hacker et al.*, 2003b], one might expect an arc-by-arc correlation between the postarc slab H₂O flux delimited in Figure 10e and the moment release of intermediate-depth earthquakes or the maximum depth of intermediate or deep seismicity. *Kirby et al.* [1996] showed a correlation between slab thermal parameter and maximum depth of seismicity. I used *Syracuse and Abers's* [2006] summary of subduction zone seismicity to evaluate whether the maximum depth of seismicity is correlated to the postarc slab H₂O flux. The data sets show no significant correlation ($r < 0.26$).

4.3. Implications for Hydrosphere Cycling

[41] What is the relationship between the postarc slab H₂O flux and the volume of H₂O within the hydrosphere and mantle? Is the postarc flux so large that significant fractions of the H₂O in Earth's H₂O reservoirs have passed through the subduction process? The hydrosphere currently comprises ~1.4E12 Tg of H₂O [*Berner and Berner*, 1987]. The calculated global postarc slab H₂O flux of 9E8 Tg/Ma yields a cycle time for the hydrosphere of 1.6 Ga, indicating that, on average, all the H₂O in the hydrosphere has passed beneath an arc volcano. *Ohtani* [2005] and *Iwamori* [2007] estimated that the mass of H₂O in the mantle is 4.5–9 times larger than that of the oceans, indicating a postarc cycle time for mantle H₂O of 7–14 Ga. These cycle times are compromised by variations in many parameters (including the rate of mantle degassing, rate of continental growth, spreading rates, average age of subducting slabs, and volume of subducting sediments [e.g., *McGovern and Schubert*, 2005; *Jarrard*, 2003; *Rüpke et al.*, 2004]) over the lifetime of Earth.

4.4. Limitations and Directions for Future Work

[42] This study necessarily has many limitations. A wide range of parameters have been used as input for the model; some of these parameters are rather poorly known and a different set of assumptions could yield substantially different outcomes. The two most uncertain parameters are the degree and

style of oceanic hydration (including hydration at spreading centers, off axis, and at outer rises) and the rate at which continental crust is subducted. Somewhat better known, perhaps, but still incompletely known are rates of subduction erosion. The *Plank and Langmuir* [1998] data set of subducted sediments is also incomplete because it is based exclusively on drill cores and therefore does not cover every subduction zone. Neither melting nor hydration of the mantle wedge were considered in the present model. Nominally anhydrous phases were not considered, yet *Iwamori* [2007] estimated that wedge mantle carried down with the subducting slab carries 1–8E8 Tg/Ma H₂O into the deep mantle. Further work refining these input parameters is encouraged.

5. Conclusions

[43] Phase diagrams were calculated for pressures of 0.5–4.0 GPa and temperatures of 300–900°C for a range of bulk compositions appropriate to subduction zones using *Perple_X*. A model for global H₂O flux at postarc depths was produced by merging these calculations with global subduction zone rock fluxes. As a very general, but useful, rule, the amount of H₂O subducted to postarc depths in hot slabs is proportional to the K₂O content of the bulk rock.

[44] The types of rock best suited for carrying H₂O to postarc depths in cold slabs are terrigenous sediment and metasomatized igneous crust; the equivalents for hot slabs are metasomatized volcanic rocks and subducted continental crust. The types of rock or subduction process most important globally in carrying H₂O to postarc depths are more difficult to define because many input parameters are poorly constrained; the present model supports suggestions that altered oceanic gabbro and peridotite dominate the global postarc slab H₂O flux, principally because these rocks are in the cold core of the slab. For any given rock type or subduction process, an arc-by-arc comparison is more fruitful because fewer unknown parameters are at play. Thus the principal suppliers of pelagic and terrigenous sediment hosted H₂O to postarc depths are the Andes and Java-Sumatra-Andaman slabs. The greatest H₂O flux from subducted continental and oceanic forearcs comes from the Chile and Solomon arcs, respectively. Subduction of hydrated ocean crust and mantle has its biggest influence on the postarc slab H₂O flux in the Andean arc.

[45] No correlations were found between postarc slab H₂O flux and characteristics of subduction zone seismicity. The global postarc slab H₂O flux is large enough that the entire hydrosphere, but only a small fraction of the mantle H₂O reservoir, could have passed through a subduction zone during the lifetime of Earth.

Acknowledgments

[46] This work was supported by NSF grants EAR-0215641 and 0510453. Thanks to Hubert Staudigel for the invitation to the GERM conference that spawned this paper, Peter van Keken for sharing the results of thermal models, Peter Cliff for suggestions regarding trench sediment compositions and sharing data tables, Jamie Connolly for *Perple_X* me, Terry Plank for spotting a hideous gaffe and sharing data tables, Dave Scholl for stimulating discussions on subduction erosion, and Doug Wilson and Jeff Karson for suggestions regarding the age and alteration of oceanic plates. This paper was reviewed by Gray Bebout, Richard Jarrard, Scott Johnston, Horst Marschall, Aral Okay, Emily Peterman, and an anonymous G-Cubed reviewer.

References

- Abers, G. A. (2005), Seismic low-velocity layer at the top of subducting slabs: Observations, predictions, and systematics, *Phys. Earth Planet. Inter.*, *149*, 7–29.
- Banerjee, N. R., K. M. Gillis, and K. Muehlenbachs (2000), Discovery of epidotes in a modern oceanic setting, the Tonga forearc, *Geology*, *28*, 151–154.
- Bebout, G. E. (1995), The impact of subduction-zone metamorphism on mantle-ocean chemical cycling, *Chem. Geol.*, *126*, 191–218.
- Berner, E. K., and R. A. Berner (1987), *The Global Water Cycle*, 397 pp., Prentice-Hall, Englewood Cliffs, N. J.
- Burtman, V. S., and P. Molnar (1993), Geological and geophysical evidence for deep subduction of continental crust beneath the Pamir, *Spec. Pap. Geol. Soc. Am.*, *281*, 1–76.
- Canales, J. P., R. S. Detrick, J. Lin, J. A. Collins, and D. R. Toomey (2000), Crustal and upper mantle seismic structure beneath the rift mountains and across a nontransform offset at the Mid-Atlantic Ridge (35°N), *J. Geophys. Res.*, *105*(B2), 2699–2720.
- Carlson, R. L. (2003), Bound water content of the lower oceanic crust estimated from modal analyses and seismic velocities of oceanic diabase and gabbro, *Geophys. Res. Lett.*, *30*(22), 2142, doi:10.1029/2003GL018213.
- Chatterjee, N. D., and E. Froese (1975), A thermodynamic study of the pseudobinary join muscovite–paragonite in the system KAlSi₃O₈–NaAlSi₃O₈–Al₂O₃–SiO₂–H₂O, *Am. Mineral.*, *60*, 985–993.
- Chopin, C. (2003), Ultrahigh-pressure metamorphism: tracing continental crust into the mantle, *Earth Planet. Sci. Lett.*, *212*, 1–14.
- Cliff, P., and P. Vannucchi (2004), Controls on tectonic accretion versus erosion in subduction zones: Implications for the origin and recycling of the continental crust, *Rev. Geophys.*, *42*, RG2001, doi:10.1029/2003RG000127.

- Connolly, J. A. D. (2005), Computation of phase equilibria by linear programming: A tool for geodynamic modeling and its application to subduction zone decarbonation, *Earth Planet. Sci. Lett.*, *236*, 524–541.
- Connolly, J. A. D., and D. M. Kerrick (2002), Metamorphic controls on seismic velocity of subducted oceanic crust at 100–250 km depth, *Earth Planet. Sci. Lett.*, *204*, 61–74.
- Connolly, J. A. D., and K. Petrini (2002), An automated strategy for calculation of phase diagram sections and retrieval of rock properties as a function of physical conditions, *J. Metamorph. Geol.*, *20*, 697–798.
- Connolly, J. A. D., and V. Trommsdorff (1991), Petrogenetic grids for metacarbonate rocks—Pressure-temperature phase-diagram projection for mixed-volatile systems *Contribut. Mineral. Petrol.*, *108*, 93–105.
- Contreras-Reyes, E., I. Grevemeyer, E. R. Flueh, M. Scherwath, and M. Heesemann (2007), Alteration of the subducting oceanic lithosphere at the southern central Chile trench—outer rise, *Geochem. Geophys. Geosyst.*, *8*, Q07003, doi:10.1029/2007GC001632.
- DeMets, C., R. G. Gordon, D. F. Argus, and S. Stein (1994), Effect of recent revisions to the geomagnetic reversal time-scale of estimates of current plate motions, *Geophys. Res. Lett.*, *21*, 2191–2194.
- Dick, H. J. B., et al. (2000), A long in situ section of the lower ocean crust: Results of ODP Leg 176 drilling at the Southwest Indian Ridge, *Earth Planet. Sci. Lett.*, *179*, 31–51.
- Ferry, J. M. (1982), A comparative geochemical study of pelitic schists and metamorphosed carbonate rocks from south-central Maine, USA, *Contrib. Mineral. Petrol.*, *80*, 59–72.
- Fuhrman, M. L., and D. H. Lindsley (1988), Ternary-feldspar modeling and thermometry, *Am. Mineral.*, *73*, 201–215.
- Grevemeyer, I., C. R. Ranero, E. R. Flueh, D. Kläschen, and J. Bialas (2007), Passive and active seismological study of bending-related faulting and mantle serpentinization at the Middle America trench, *Earth Planet. Sci. Lett.*, *258*, 528–542.
- Grove, T. L., N. Chatterjee, S. W. Parman, and E. Medard (2006), The influence of H₂O on mantle wedge melting, *Earth Planet. Sci. Lett.*, *249*(1–2), 74–89.
- Gunn, B. M., and M. J. Roobol (1977), Geochemistry of the igneous rocks, *Initial Rep. Deep Sea Drill. Proj.*, *37*, 735–755.
- Hacker, B. R. (2007), Ascent of the ultrahigh-pressure Western Gneiss Region, Norway, in *Convergent Margin Terranes and Associated Regions: A Tribute to W. G. Ernst*, edited by M. Cloos et al., *Spec. Pap. Geol. Soc. Am.*, *419*, 171–184.
- Hacker, B. R., and G. A. Abers (2004), Subduction Factory 3: An Excel worksheet and macro for calculating the densities, seismic wave speeds, and H₂O contents of minerals and rocks at pressure and temperature, *Geochem. Geophys. Geosyst.*, *5*, Q01005, doi:10.1029/2003GC000614.
- Hacker, B. R., L. Ratschbacher, L. E. Webb, M. McWilliams, T. R. Ireland, A. Calvert, S. Dong, H.-R. Wenk, and D. Chateigner (2000), Exhumation of ultrahigh-pressure continental crust in east-central China: Late Triassic–Early Jurassic tectonic unroofing, *J. Geophys. Res.*, *105*, 13,339–13,364.
- Hacker, B. R., G. A. Abers, and S. M. Peacock (2003a), Subduction factory 1. Theoretical mineralogy, densities, seismic wave speeds, and H₂O contents, *J. Geophys. Res.*, *108*(B1), 2029, doi:10.1029/2001JB001127.
- Hacker, B. R., S. M. Peacock, and G. A. Abers (2003b), Subduction factory 2. Are intermediate-depth earthquakes in subducting slabs linked to metamorphic dehydration reactions?, *J. Geophys. Res.*, *108*(B1), 2030, doi:10.1029/2001JB001129.
- Hacker, B. R., P. Luffi, V. Lutkov, V. Minaev, L. Ratschbacher, T. Plank, M. Ducea, A. Patiño-Douce, M. McWilliams, and J. Metcalf (2005), Near-ultrahigh pressure processing of continental crust: Miocene crustal xenoliths from the Pamir, *J. Petrol.*, *46*, 1661–1687.
- Hilton, D. R., T. P. Fischer, and B. Marty (2002), Noble gases and volatile recycling at subduction zone, in *Noble Gases in Cosmochemistry and Geochemistry, Reviews in Mineralogy and Geochemistry*, edited by D. Porcelli, C. J. Ballentine, and R. Wieler, pp. 319–370, Mineral. Soc. of Am., Chantilly, Va.
- Holland, T., and R. Powell (1996), Thermodynamics of order-disorder in minerals; II, Symmetric formalism applied to solid solutions, *Am. Mineral.*, *81*, 1425–1437.
- Holland, T. J. B., and R. Powell (1998), An internally consistent thermodynamic data set for phases of petrological interest, *J. Metamorph. Geol.*, *16*, 309–343.
- Holland, T., J. Baker, and R. Powell (1998), Mixing properties and activity-composition relationships of chlorites in the system MgO-FeO-Al₂O₃-SiO₂-H₂O, *Earth Planet. Sci. Lett.*, *10*, 395–406.
- Ito, E., D. M. Harris, and A. T. Anderson (1983), Alteration of oceanic crust and geologic cycling of chlorine and water, *Geochim. Cosmochim. Acta*, *47*, 1613–1624.
- Iwamori, H. (2007), Transportation of H₂O beneath the Japan arcs and its implications for global water circulation, *Chem. Geol.*, *239*, 182–198.
- Jarrard, R. D. (2003), Subduction fluxes of water, carbon dioxide, chlorine, and potassium, *Geochem. Geophys. Geosyst.*, *4*(5), 8905, doi:10.1029/2002GC000392.
- Johnson, M. R. W. (2002), Shortening budgets and the role of continental subduction during the India-Asia collision, *Earth Sci. Rev.*, *59*, 101–123.
- Johnston, S. (2006), The evolution of the Nordfjord-Sogn detachment zone and the exhumation of Norwegian ultrahigh-pressure rocks, Ph.D. thesis, Univ. of Calif., Santa Barbara.
- Karson, J. (1998), Internal structure of oceanic lithosphere: A perspective from tectonic windows, in *Faulting and Magmatism at Mid-Ocean Ridges*, *Geophys. Monogr. Ser.*, vol. 106, edited by W. R. Buck et al., pp. 177–217, AGU, Washington, D. C.
- Kelemen, P. B., et al. (2004), *Drilling Mantle Peridotite Along the Mid-Atlantic Ridge From 14° to 16°N*, *Proceedings of the Ocean Drilling Program, Initial Reports*, vol. 209, Ocean Drilling Program, College Station, Tex.
- Kerrick, D. M., and J. A. D. Connolly (2001a), Metamorphic devolatilization of subducted marine sediments and the transport of volatiles into the Earth's mantle, *Nature*, *411*, 293–296.
- Kerrick, D. M., and J. A. D. Connolly (2001b), Metamorphic devolatilization of subducted oceanic metabasalts: Implications for seismicity, arc magmatism and volatile recycling, *Earth Planet. Sci. Lett.*, *189*, 19–29.
- Kirby, S. H., W. B. Durham, and L. A. Stern (1991), Mantle phase changes and deep-earthquake faulting in subducting lithosphere, *Science*, *252*, 216–225.
- Kirby, S. H., E. R. Engdahl, and R. Denlinger (1996), Intermediate-depth intraslab earthquakes and arc volcanism as physical expressions of crustal and uppermost mantle metamorphism in subducting slabs, in *Subduction: Top to Bottom*, *Geophys. Monogr. Ser.*, vol. 96, edited by G. E. Bebout, D. Scholl, and S. Kirby, pp. 195–214, AGU, Washington, D. C.
- Lallemand, S., A. Heuret, and D. Boutelier (2005), On the relationships between slab dip, back-arc stress, upper plate

- absolute motion, and crustal nature in subduction zones, *Geochem. Geophys. Geosyst.*, **6**, Q09006, doi:10.1029/2005GC000917.
- Liou, J. G., T. Tsujimori, R. Y. Zhang, I. Katayama, and S. Maruyama (2004), Global UHP metamorphism and continental subduction/collision: The Himalayan model, *Int. Geol. Rev.*, **46**, 1–27.
- McGovern, P. J., and G. Schubert (2005), Thermal evolution of the Earth: Effects of volatile exchange between atmosphere and interior, *Earth Planet. Sci. Lett.*, **96**, 27–37.
- Newton, R. C., T. V. Charlu, and O. J. Kleppa (1980), Thermochimistry of the high structural state plagioclases, *Geochim. Cosmochim. Acta*, **44**, 933–941.
- Ohtani, E. (2005), Water in the mantle, *Elements*, **1**, 25–30.
- Patiño Douce, A. E. (2005), Vapor-absent melting of tonalite at 15–32 kbar, *J. Petrol.*, **46**, 275–290.
- Peacock, S. M. (1990), Fluid processes in subduction zones, *Science*, **248**, 329–337.
- Peacock, S. M. (2001), Are the lower planes of double seismic zones caused by serpentine dehydration in subducting oceanic mantle?, *Geology*, **29**, 299–302.
- Pearce, J. A. (1976), Statistical analysis of major element patterns in basalts, *J. Petrol.*, **17**, 15–43.
- Plank, T., and C. H. Langmuir (1998), The chemical composition of subducting sediment and its consequences for the crust and mantle, *Chem. Geol.*, **145**, 325–394.
- Plank, T., K. A. Kelley, R. W. Murray, and L. Q. Stern (2007), Chemical composition of sediments subducting at the Izu-Bonin trench, *Geochem. Geophys. Geosyst.*, **8**, Q04I16, doi:10.1029/2006GC001444.
- Poli, S., and M. W. Schmidt (2002), Petrology of subducted slabs, *Annu. Rev. Earth Planet. Sci.*, **30**, 207–235.
- Powell, R., and T. Holland (1999), Relating formulations of the thermodynamics of mineral solid solutions; activity modeling of pyroxenes, amphiboles, and micas, *Am. Mineral.*, **84**, 1–14.
- Ranero, C. R., and V. Sallares (2004), Geophysical evidence for hydration of the crust and mantle of the Nazca Plate during bending at the north Chile Trench, *Geology*, **32**(7), 549–552.
- Ranero, C. R., T. J. Reston, I. Belykh, and H. G. Nibidenko (1997), Reflective oceanic crust formed at a fast-spreading center in the Pacific, *Geology*, **25**, 499–502.
- Ranero, C. R., A. Villasenor, J. Phipps Morgan, and W. Weinrebe (2005), Relationship between bend-faulting at trenches and intermediate-depth seismicity, *Geochem. Geophys. Geosyst.*, **6**, Q12002, doi:10.1029/2005GC000997.
- Reilinger, R., et al. (2006), GPS constraints on continental deformation in the Africa-Arabia-Eurasia continental collision zone and implications for the dynamics of plate interactions, *J. Geophys. Res.*, **111**, B05411, doi:10.1029/2005JB004051.
- Rüpke, L. H., J. P. Morgan, and J. A. D. Connolly (2004), Serpentine and the subduction zone water cycle, *Earth Planet. Sci. Lett.*, **223**, 17–34.
- Rüpke, L., J. P. Morgan, and J. E. Dixon (2006), Implications of subduction rehydration for Earth's deep water cycle, in *Earth's Deep Water Cycle*, *Geophys. Monogr. Ser.*, vol. 168, edited by S. D. Jacobsen and S. van der Lee, pp. 263–276, AGU, Washington, D. C.
- Schmidt, M. W., and S. Poli (1998), Experimentally based water budgets for dehydrating slabs and consequences for arc magma generation, *Earth Planet. Sci. Lett.*, **163**, 361–379.
- Schmidt, M. W., and S. Poli (2003), Generation of mobile components during subduction of oceanic crust, in *Treatise on Geochemistry*, vol. 3, *The Crust*, edited by R. Rudnick, pp. 567–591, Elsevier, New York.
- Schmidt, M. W., D. Vielzeuf, and E. Auzanneau (2004), Melting and dissolution of subducting crust at high pressures: The key role of white mica, *Earth Planet. Sci. Lett.*, **228**, 65–84.
- Scholl, D. W., and R. von Huene (2008), Crustal recycling at modern subduction zones applied to the past—Issues of growth and preservation of continental basement, mantle geochemistry, and supercontinent reconstruction, in *The 4D Framework of Continental Crust*, edited by Robert D. Hatcher, Jr. et al., *Spec. Pap. Geol. Soc. Am.*, in press.
- Searle, M., B. R. Hacker, and R. Bilham (2001), The Hindu Kush seismic zone as a paradigm for the creation of ultrahigh-pressure diamond and coesite-bearing rocks, *J. Geol.*, **109**, 143–154.
- Seno, T., and Y. Yamanaka (1996), Double seismic zones, compressional deep trench-outer rise events, and superplumes, in *Subduction: Top to Bottom*, *Geophys. Monogr. Ser.*, vol. 96, edited by G. E. Bebout et al., pp. 347–355, AGU, Washington, D. C.
- Smith, W. H. F., and D. T. Sandwell (1997), Global seafloor topography from satellite altimetry and ship depth soundings, *Science*, **277**, 1957–1962.
- Snow, J. E., and H. J. B. Dick (1995), Pervasive magnesium loss by marine weathering of peridotite, *Geochim. Cosmochim. Acta*, **59**, 4219–4235.
- Staudigel, H., T. Plank, B. White, and H.-R. Schminke (1996), Geochemical fluxes during seafloor alteration of the basaltic upper oceanic crust: DSDP Sites 417 and 418, in *Subduction: Top to Bottom*, *Geophys. Monogr. Ser.*, vol. 96, edited by G. E. Bebout et al., pp. 19–37, AGU, Washington, D. C.
- Stern, C. R., W. L. Huang, and P. J. Wyllie (1975), Basalt-andesite-rhyolite-H₂O: Crystallization intervals with excess H₂O and H₂O-undersaturated liquidus surfaces to 35 kilobars, with implications for magma genesis, *Earth Planet. Sci. Lett.*, **28**, 189–196.
- Syracuse, E. M., and G. A. Abers (2006), Global compilation of variations in slab depth beneath arc volcanoes and implications, *Geochem. Geophys. Geosyst.*, **7**, Q05017, doi:10.1029/2005GC001045.
- Tesauro, M., C. Hollenstein, R. Egli, A. Geiger, and H.-G. Kahle (2005), Continuous GPS and broad-scale deformation across the Rhine Graben and the Alps, *Int. J. Earth Sci.*, **94**(4), 525–537.
- Thompson, J. B., and G. L. Hovis (1979), Entropy of mixing in sanidine, *Am. Mineral.*, **64**, 57–65.
- Vielzeuf, D., and M. W. Schmidt (2001), Melting relations in hydrous systems revisited: Application to metapelites, metagraywackes and metabasalts, *Contrib. Mineral. Petrol.*, **141**, 251–267.
- von Huene, R., and D. W. Scholl (1991), Observations at convergent margins concerning sediment subduction, subduction erosion, and the growth of continental crust, *Rev. Geophys.*, **29**, 279–316.
- Wallmann, K. (2001), The geological water cycle and the evolution of marine $\delta^{18}\text{O}$ values, *Geochim. Cosmochim. Acta*, **65**(15), 2469–2485.
- Walsh, E. O., and B. R. Hacker (2004), The fate of subducted continental margins: Two-stage exhumation of the high-pressure to ultrahigh-pressure Western Gneiss complex, Norway, *J. Metamorph. Geol.*, **22**, 671–689.
- Wei, C., and R. Powell (2003), Phase relations in high-pressure metapelites in the system KFMASH (K₂O-FeO-MgO-Al₂O₃-SiO₂-H₂O) with application to natural rocks, *Contrib. Mineral. Petrol.*, **145**, 301–315.

- White, R. W., R. Powell, T. J. B. Holland, and B. Worley (2000), The effect of TiO₂ and Fe₂O₃ on metapelitic assemblages at greenschist and amphibolite facies conditions: Mineral equilibria calculations in the system K₂O-FeO-MgO-Al₂O₃-SiO₂-H₂O-TiO₂-Fe₂O₃, *J. Metamorph. Geol.*, *18*, 497–511.
- White, R. W., R. Powell, and G. N. Phillips (2003), A mineral equilibria study of the hydrothermal alteration in mafic greenschist facies rocks at Kalgoorlie, Western Australia, *J. Metamorph. Geol.*, *21*, 455–468.
- Wilson, M. (1989), *Igneous Petrogenesis*, 466 pp., Unwin Hyman, Boston, Mass.
- Workman, R. K., and S. R. Hart (2005), Major and trace element composition of the depleted MORB mantle (DMM), *Earth Planet. Sci. Lett.*, *231*, 53–72.